Ore Geology Reviews xxx (2008) xxx–xxx

Contents lists available at ScienceDirect

Ore Geology Reviews

journal homepage: www.elsevier.com/locate/oregeorev

Thrust-controlled, sediment-hosted, Himalayan Zn–Pb–Cu–Ag deposits in the Lanping foreland fold belt, eastern margin of Tibetan Plateau

Longqing He [a], Yucai Song [b], Kaixu Chen [a], Zengqian Hou [b,*], Fengming Yu [a], Zhusen Yang [c], Junqi Wei [a], Zheng Li [b], Yingchao Liu [c]

[a] Yichang Institute of Geology and Mineral Resources, Yichang 443003, PR China
[b] Institute of Geology, Chinese Academy of Geological Sciences, 26 Baiwanzhuang Road, Beijing 100037, PR China
[c] Institute of Mineral Resources, Chinese Academy of Geological Sciences, Beijing 10003, PR China

ARTICLE INFO

Article history:
Received 22 January 2008
Received in revised form 6 October 2008
Accepted 5 November 2008
Available online xxxx

Keywords:
Lanping
Zn–Pb–Cu–Ag deposit
Thrust system
Basinal brines
Himalayan

ABSTRACT

Cenozoic economic Zn–Pb–Cu–Ag ore deposits occur in the Lanping foreland fold belt (Lanping basin) of the Eastern Indo-Asian collision zone (EIACZ), eastern margin of the Tibetan plateau. They are sediment-hosted and controlled by two Cenozoic thrust–nappe systems developed in the western and eastern segments of the Tertiary basin, respectively, where thrusting was towards the centre of the basin in an approximately E–W direction and juxtaposes Triassic–Cretaceous over Tertiary strata.

In the western system, Cu deposits occur as veins in the root zone, hosted by ~NS-striking faults in Jurassic intense folds. Zn deposits occur in its front zone, controlled by second-order faults of major thrust faults and thrust-related strike-slip faults. In the eastern system, Zn–Pb–Cu–Ag deposits are located in the front zone, controlled by an E-dipping thrust fault and its second-order faults. The giant Jinding Zn–Pb deposit is controlled by a trap structure related to regional thrusting.

Homogenization temperatures of fluid inclusions from these deposits are predominately <200 °C, with salinities of 1.6 to 27.7 wt.% NaCl equiv. Ore sulfides have Pb isotopes similar to the rocks in the basin and $\delta^{34}S_{CDT}$ values ranging from −30.4‰ to 11.2‰. H–O isotopes of fluid inclusions are similar to those of basinal brines, and C–O isotopes of hydrothermal carbonate minerals are partly close to those of carbonates and sedimentary organisms. These data suggest that the ore-forming fluids and materials mainly derive from the fluids and various rocks of the basin, respectively.

The sediment-hosted Zn–Pb–Cu–Ag deposits in the Lanping foreland fold belt share some similarities with MVT-, SST-, SSC-, and SEDEX-type deposits in that there is a lack of any igneous affinity and instead must relate to activities of basinal fluids. The deposits show, however, a set of unique features: (1) they were formed in a strongly deformed foreland basin within a continent collision orogen and (2) closely related to regional thrust–nappe structure; (3) they are fault-controlled, commonly without strong selection for type of host rocks; and (4) contain a variety of metals including Zn, Pb, Cu, Ag, and minor Sr, Co, etc. It is suggested that the Zn–Pb–Cu–Ag deposits controlled by the thrust systems in the Lanping foreland belt are a new sub-type within the family of sediment-hosted base metal deposits.

1. Introduction

Worldwide, four principle classes of sediment-hosted base metal deposits have been recognized: sedimentary exhalative (SEDEX) Zn–Pb; Mississippi Valley-type (MVT) Zn–Pb; sandstone-type (SST) Pb–Zn; and sandstone-hosted Cu (SSC) deposits. All these deposit types generally have no obvious genetic association with igneous activity and were formed from basinal fluids during the normal evolution of the basins (Misra, 2000). In the last decades, numerous models for these deposits have been developed (Bjørlykke and Sangster, 1981; Sangster, 1990; Pirajno, 1992; Misra, 2000; Leach et al., 2005), providing important guidelines for exploration of these deposits.

It is difficult, however, to use these existing models to describe and explain the Himalayan sediment-hosted Zn–Pb–Cu–Ag ore-forming systems in the eastern Indo-Asian collision zone (EIACZ), which produced numerous economically significant deposits. These deposits all occur in the Lanping foreland fold belt and include the giant Jinding Zn–Pb deposit (Shi et al., 1983; Qin and Zhu, 1991; Luo et al., 1994; Li and Kyle, 1997; Kyle and Li, 2002; Xue et al., 2007), the Sanshan Zn–Pb–Ag–Cu deposit (Gong et al., 2000; Chen et al., 2000, 2004; Yang, 2002; Yang et al., 2003), the Fulongchang Zn–Pb–Ag–Cu deposit (Tian, 1997; Chen et al., 2004; He et al., 2006), and the Jinman Cu deposit, etc. (Yan and Li, 1997; Ji and Li, 1998; Liu et al., 2001; Gao et al., 2006). They were formed in the strongly deformed Tertiary foreland basin within a Cenozoic active

* Corresponding author. Tel.: +86 10 68990617; fax: +86 10 68997803.
E-mail address: Houzengqian@126.com (Z. Hou).

0169-1368/$ – see front matter © 2008 Elsevier B.V. All rights reserved.
doi:10.1016/j.oregeorev.2008.11.001

collisional setting (Hou et al., 2006, 2007; Xue et al., 2007), and are strictly controlled by the Cenozoic thrust systems related to Indo-Asian collision since the Paleocene (Xu and Li, 2003; He et al., 2004a; Xu and Zhou, 2004). These distinctions clearly set them apart from other types of sediment-hosted base metal deposit. For example, MVT deposits are mainly formed in mildly deformed or undeformed sedimentary basins in foreland or continental rift environments, whereas SST, SSC, and SEDEX deposits were usually formed in sedimentary basins in stable or extensional settings (Misra, 2000; Leach et al., 2005). The relatively clear tectonic setting, young age of ore formation, giant metallic endowment, and weak reworking of those deposits provides an opportunity to understand the metallogenesis of the Zn–Pb–Cu–Ag ore-forming systems in continental collisional settings.

This paper aims to analyze the Cenozoic thrust–nappe systems and the geology of the main deposits. Existing and new fluid inclusion data and Pb, S, H–O, and C–O isotope studies of the Zn–Pb–Cu–Ag deposits in the foreland fold belt are also summarized. We also discuss and roles of the thrust–nappe system in ore formation, the age of mineralization, and sources of ore-forming fluids and materials. Finally, we make a detailed comparison of the deposits of the Lanping belt with MVT, SST, SSC, and SEDEX deposits.

2. Regional geology and tectonic setting

The Lanping-Simao foreland fold belt (Fig. 1), in which the Himalayan Zn–Pb–Cu–Ag ore-forming systems were developed, is tectonically located in the eastern Indo-Asian collision zone (EIACZ), the eastern margin of the Tibetan plateau (Fig. 1). The EIACZ, characterized by high topographic relief, is bounded by a series of NW-striking Cenozoic strike-slip fault systems (Fig. 1). The Lanping Basin (Fig. 2) in the EIACZ underwent a complex history of tectonic evolution from late Triassic rifting, Jurassic–Cretaceous depression, early Tertiary foreland development, and finally incorporation as part of the Lanping-Simao foreland fold belt (Wang et al., 2001), as a consequence of eastern Tibetan crustal shortening related to Indo-Asian collision (Wang and Burchfiel, 1997).

2.1. Basin evolution

A three-stage tectonic evolution for the Lanping complex basin can be established based on numerous studies (Liu et al., 1983; Li et al., 1999; Mu et al., 1999; Pan et al., 2003; He et al., 2004a) and the 1:200,000 geological maps of western Yunnan.

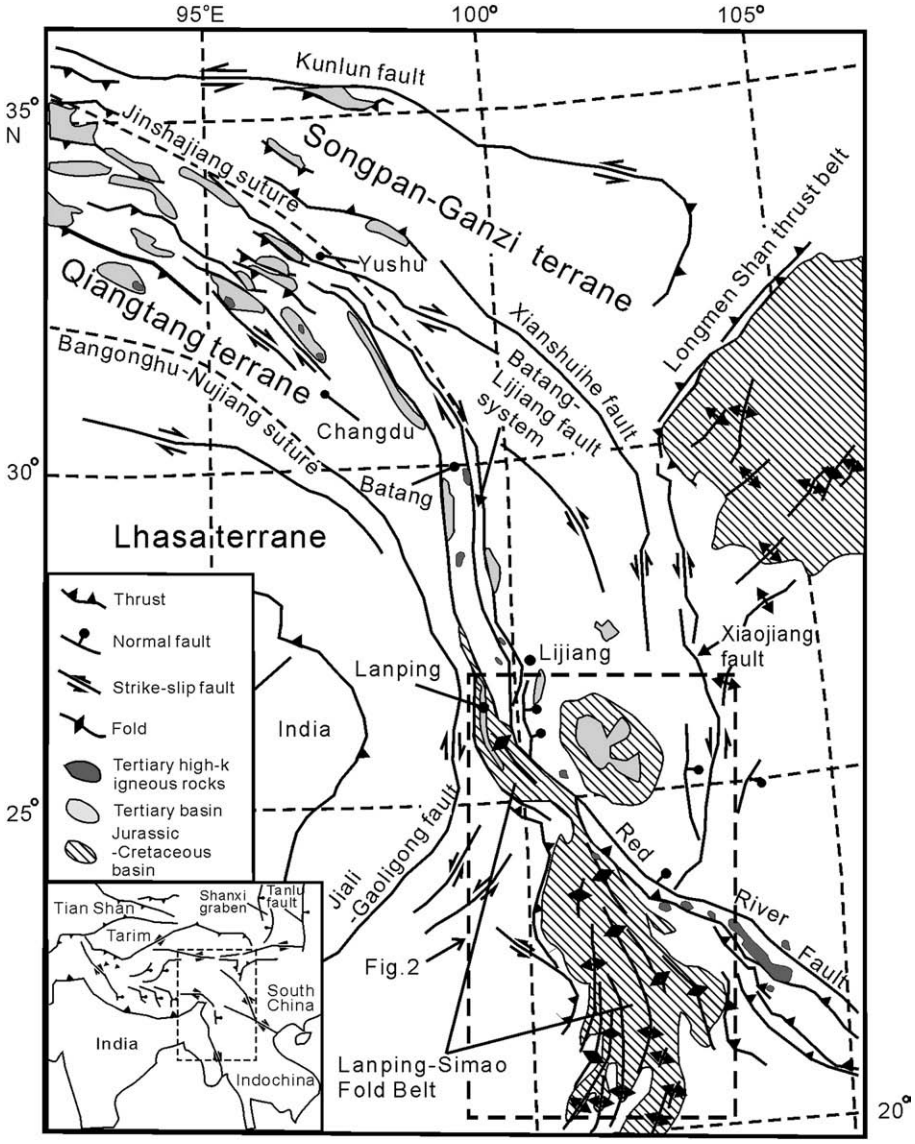

Fig. 1. Cenozoic tectonic map of eastern Tibet and Indochina, showing the structure systems and the distribution of Mesozoic to Cenozoic basins (modified from Wang et al., 2001).

Please cite this article as: He, L., et al., Thrust-controlled, sediment-hosted, Himalayan Zn–Pb–Cu–Ag deposits in the Lanping foreland fold belt, eastern margin of Tibetan Plateau, Ore Geology Reviews (2008), doi:10.1016/j.oregeorev.2008.11.001

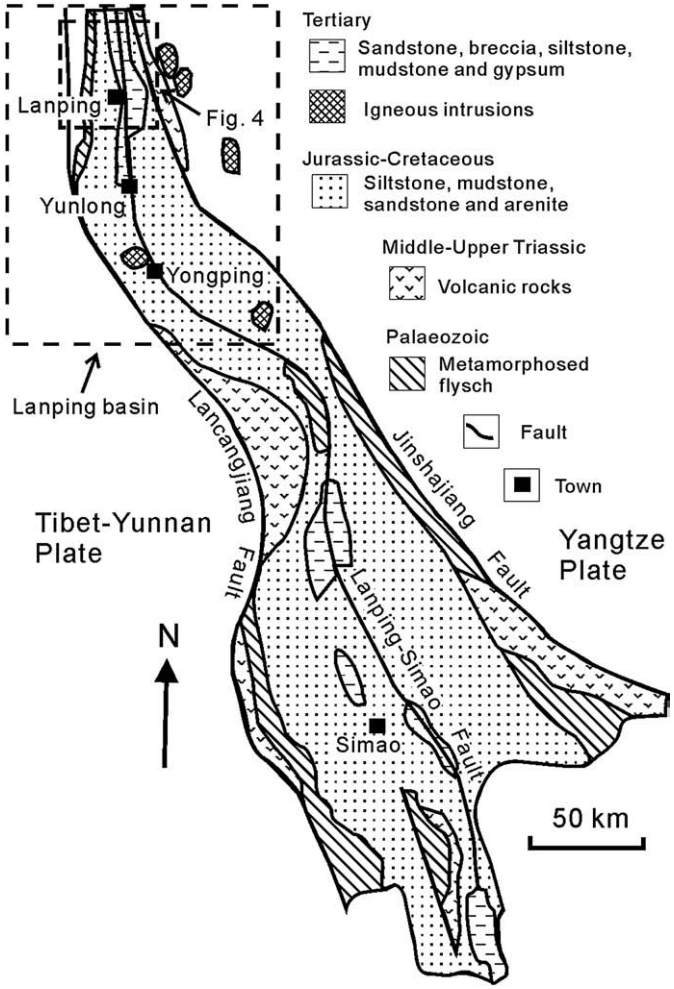

Fig. 2. Sketch geological map of the Lanping-Simao fold belt, showing the major structures and the distribution of the rocks (after Xue et al., 2007). The location is shown in Fig. 1.

2.1.1. Late-Triassic rift basin

The rift basin was developed in the Changdu-Simao continental block, bounded by the Lancangjiang and the Jinshajiang faults (sutures) (Fig. 2), representatives of Paleo-Tethyan ocean relicts (Liu et al., 1993; Mo et al., 1993; Li et al., 1999). Subduction of both oceanic-slabs in the Late Permian resulted in the development of the continental margin arcs and associated Triassic arc volcanic-sedimentary sequences along both edges of the continental block (Mo et al., 1993). Subsequently, arc-continent (block) collision caused closure of the oceanic basins in the Early Triassic (Li et al., 1999) and eruption of middle-Triassic syn-collisional volcanic rocks in both arcs (Mo et al., 1993). Post-collisional extension, beginning in the Middle to Late Triassic, triggered bimodal volcanism along the volcanic arcs (Fig. 2) (Pan et al., 2003), and led to the Changdu-Simao block rifting to form the Lanping rift basin. The volcanic rocks occur in the east and west of the Lanping basin, whereas shallow marine clastics (T_3w), carbonates (T_3s) and sandy mudstone (T_3wl, T_3m) sequences (Fig. 3) filled the basin. The strata constitute a significant basement rock unit for the Tertiary foreland basin (Mu et al., 1999; Zhong et al., 2000; Liao and Chen, 2005).

2.1.2. Jurassic–Cretaceous depression basin

Associated with opening of the Bangong-Nujiang ocean in the Jurassic (Liu et al., 1993) and closure of the Garzê-Litang oceanic basin at the end of Triassic (Hou et al., 1995), over 5 km of flysch complexes in the Songpan-Garzê terrane were underthrust beneath the Changdu-Simao block (Yin and Harrison, 2000; Spurlin et al., 2005). The Lanping area thus evolved from a Triassic rift basin into a depression basin in a regional compressional regime. The basin is filled with Jurassic marine-terrestrial red clastics and minor carbonates (J_1y, J_2h, J_3b), Cretaceous shallow lake-facies sandy-mudstone, coarse-grained sandstone-arenite formations (K_1j, K_1n) and red terrestrial clastics (K_2h) (Fig. 3) (Mu et al., 1999). These fill sequences, as a basement unit of the Tertiary foreland basin, were finally juxtaposed over the Tertiary basin strata by thrusting.

2.1.3. Tertiary foreland basin

Initial impact and collision of the Indo-Asian continents at ca. 65 to 50 Ma led to development of the collisional orogen in central Tibet; associated Cenozoic contraction started prior to 51 Ma in eastern Tibet (Spurlin et al., 2005). This collision caused further contraction of the Mesozoic depression basins, which evolved into a series of isolated Tertiary foreland basins along the eastern edge of the Tibetan Plateau (Fig. 1) (Wang et al., 2001; Spurlin et al., 2005; Li et al., 2006a). The Lanping basin, one of these foreland basins, was developed within the Mesozoic depression basin and is bounded by the Jinshajiang fault to the east and by the Lanchangjiang fault to the west (Fig. 2). Mid-Proterozoic metamorphic basement rocks (sericite schist, marble, gneiss and amphibolites) outcrop along both basin-marginal faults. The Tertiary basin is filled with silicicalstic rock sequences of an isolated lake-facies basinal environment. The sequences mainly include E_1y composed of gypsum-bearing red fine-grained clastics (siltstone and mudstone) in the lower part and gypsum-bearing coarse-grained clastics (breccia and sandstone) in the upper part, E_2g composed of gypsum-bearing argillanceous sandstone, siltstone and molasse formation (Xue et al., 2002), and E_2b composed of sandstone, sandy-mudstone, and molasses formation (Fig. 3) (Mu et al., 1999). At least six evaporate horizons, dominated by gypsum with minor halite, with a local total thickness of over 2 km, have been recognized in the basin.

2.2. Cenozoic deformation

The history of Cenozoic deformation in the EIACZ can be divided into four stages: (1) Paleocene–Eocene compression (~65 to 42 Ma), (2) Eocene–Oligocene transpression (~40 to 26 Ma), (3) early-middle-Miocene transtension (~25 to 18 Ma), and (4) late-Neocene E–W extension (<18 Ma) (Wang et al., 2001; Hou et al., 2006). Paleocene–Eocene compression resulted in development of the Cenozoic contraction structures characterized by a series of thrust systems beginning at ~51 Ma (Spurlin et al., 2005) and subsequent formation of the Lanping-Simao fold belt in the EIACZ (Fig. 1) (Wang et al., 2001). In the Lanping area, these thrust systems juxtaposed the Triassic, Jurassic, and Cretaceous strata over the Tertiary basin strata (Fig. 4). The Eocene–Oligocene transpression produced a series of Cenozoic strike-slip faulting systems, such as the Jiali-Gaoligong and Batang-Lijiang strike-slip systems, the Red River fault, and the Xianshuihe fault (Fig. 1). Strike-slip faulting occurred at 40 Ma and ceased at 23 Ma (Hou et al., 2003; Liu et al., 2006), and underwent early-stage sinistral and late-stage dextral movements (Tapponnier et al., 1990; Spurlin et al., 2005). Although numerous potassic felsic stocks (~42 to 23 Ma) were developed along these strike-slip faults (Chung et al., 1998; Wang et al., 2001; Hou et al., 2003), only a few felsic stocks, with a $^{40}Ar/^{39}Ar$ age of 35 Ma, intruded the Lanping-Simao fold belt (Dong et al., 2005). These sinistral or dextral strike-slip faults commonly damaged the Eocene thrust systems, and in turn were replaced by mid-Miocene extensional structures, marked by metamorphic core-complexes in the EIACZ (Liu et al., 2006).

3. Cenozoic thrust–nappe systems

The thrust–nappe systems, a significant deformational style in the Lanping fold belt, resulted from Indo-Asian collision and subsequent

Please cite this article as: He, L., et al., Thrust-controlled, sediment-hosted, Himalayan Zn–Pb–Cu–Ag deposits in the Lanping foreland fold belt, eastern margin of Tibetan Plateau, Ore Geology Reviews (2008), doi:10.1016/j.oregeorev.2008.11.001

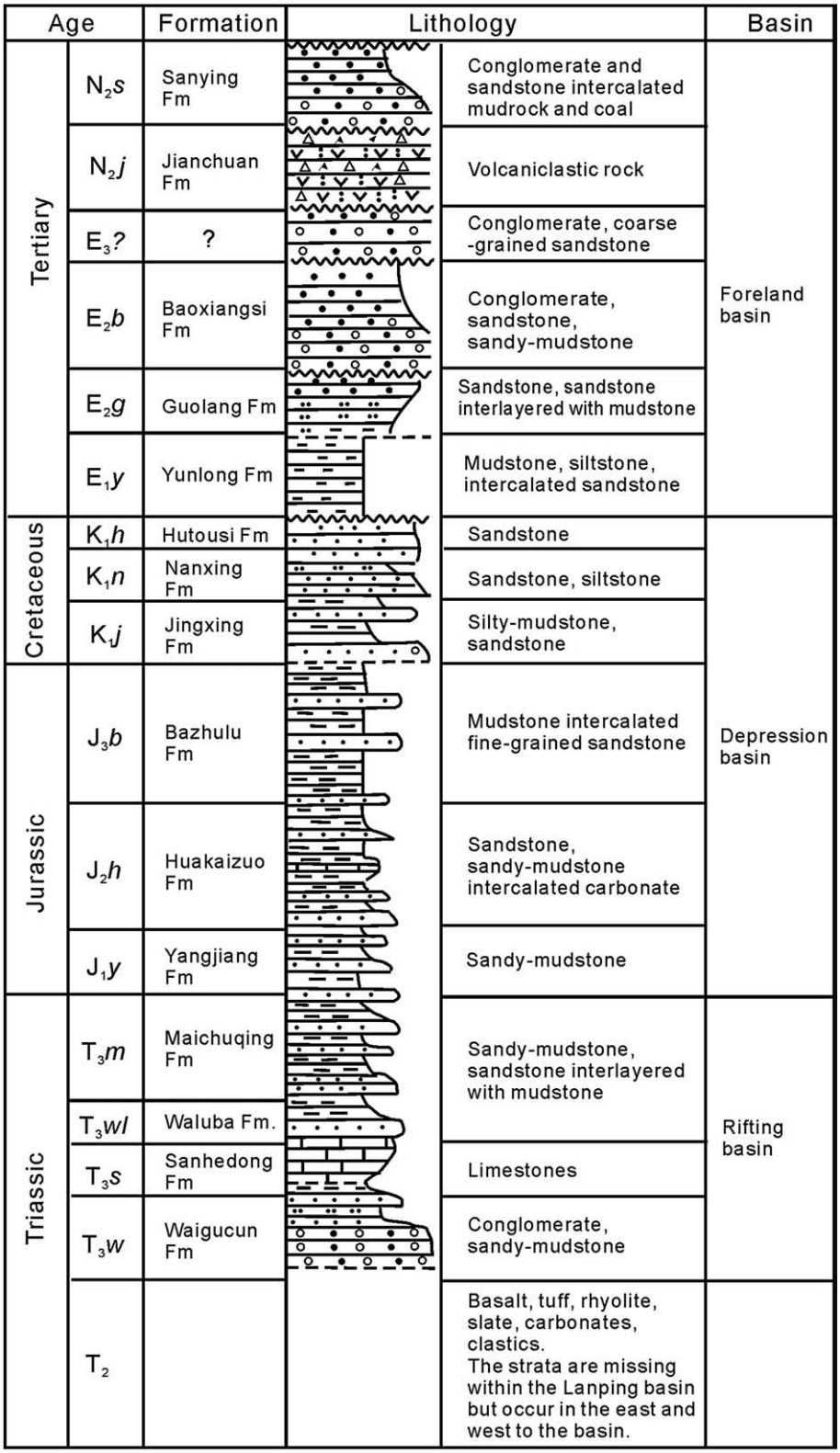

Fig. 3. Stratigraphic units in the Lanping basin (modified from Mu et al., 1999).

oblique convergence during the Paleocene to Eocene. Two approximately E–W-striking geologic cross-sections in the northern Lanping basin show that main thrust faults dip to west and to east in the western and eastern segments, respectively (Figs. 4, 5a, b); the central Tertiary strata represent the boundary. Accordingly, we identified them as two large-scale thrust–nappe systems whose thrusting was in

Please cite this article as: He, L., et al., Thrust-controlled, sediment-hosted, Himalayan Zn–Pb–Cu–Ag deposits in the Lanping foreland fold belt, eastern margin of Tibetan Plateau, Ore Geology Reviews (2008), doi:10.1016/j.oregeorev.2008.11.001

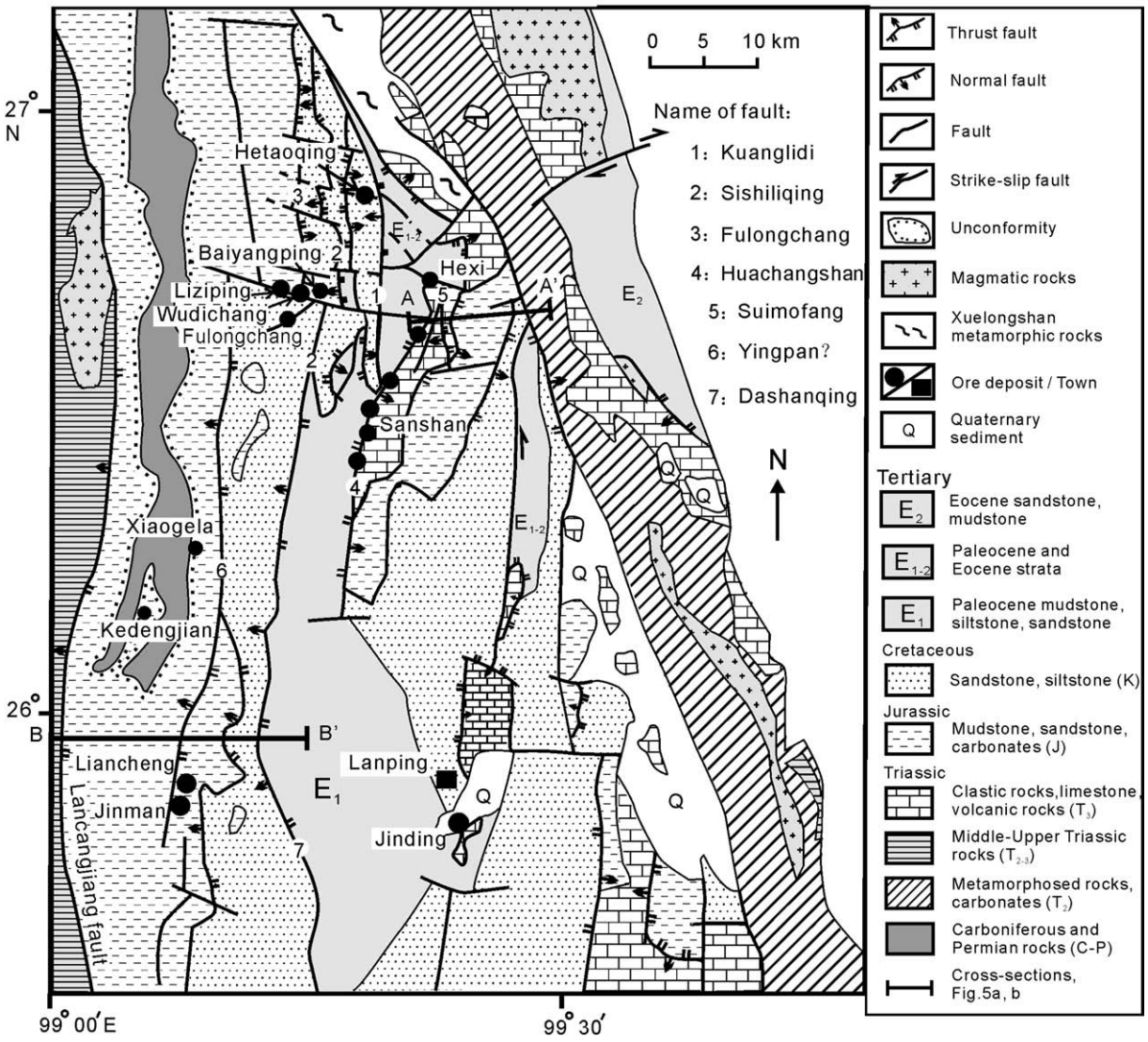

Fig. 4. Simplified geological map of the northern Lanping basin showing the distributions of stratigraphic units, faults, and major Zn–Pb–Cu–Ag ore deposits (modified from Xu and Li, 2003). The location is shown in Fig. 2.

an approximately E–W direction and ongoing towards the Tertiary strata (E_1, E_2) in the basin centre (Figs. 4, 5a, b).

3.1. Western thrust–nappe system

This mainly consists of a series of W-dipping thrust faults and the Triassic, Jurassic, and Cretaceous strata (Figs. 4, 5a). The thrust faults are commonly high-angle and the angles decrease towards the east (Fig. 5a). Older strata overlay younger strata along these faults, a consequence of eastward thrusting of the Triassic to Cretaceous strata over the Tertiary strata. The thrusting caused strong deformation of the Jurassic strata forming reverse folds (Fig. 5a); some small-scale approximately N–S-striking compressive faults are also present.

In the northern segment, the system contains (1) a series of NS-striking faults, such as the Kuanglidi, Sishiliqing, and Fulongchang faults, (2) a ca. 10 km wide zone of intense folding of the Jurassic strata, and (3) a group of high-angle ~EW-striking faults offsetting the NS-striking faults (Fig. 4). The NS-striking Kuanglidi thrust fault dips to west or southwest at variable angles, and juxtaposes Cretaceous strata over the Tertiary basinal strata (Fig. 4). The Sishiliqing thrust fault dips ~35° to west and the Fulongchang normal fault dips to east; both contain a series of NE-striking second-order faults. To the west, the intense folding made the Jurassic thrust slice form a nearly NS-striking anticlinorium in which Carboniferous-Permian strata outcrop in the core, whereas the high-angle, west-dipping, imbricate thrust faults juxtapose Middle to Upper Triassic volcanic rocks over Jurassic strata (Figs. 4, 5a). The ~EW-striking, steeply-dipping, parallel faults cut off most NS-striking faults, but are usually ended by the Kuanglidi thrust fault (Fig. 4), showing typical strike-slip faulting induced by thrusting.

3.2. Eastern thrust–nappe systems

This contains a series of E-dipping thrust and normal faults, resulted from westward thrusting of the Triassic, Jurassic, and Cretaceous strata over the Tertiary strata (Figs. 4, 5b). By analysis of the geologic cross-section in the northern segment (Fig. 5b), three structural zones were identified in the system, i.e., the front, central, and root zones (He et al., 2004a). The root zone generally consists of high-angle east-dipping faults, which juxtapose a Triassic carbonate sequence over Jurassic–Cretaceous strata (Fig. 5b). The central zone contains a 3 to 5 km wide block of Jurassic, and locally outcropping Cretaceous strata. It is bounded by two parallel, east-dipping normal faults and hosts some east-dipping thrust faults (Fig. 5b). The front zone is characterized by development of low-angle thrust faults that juxtapose Mesozoic strata over Tertiary strata (E_1y. and E_2g.). The low-

Please cite this article as: He, L., et al., Thrust-controlled, sediment-hosted, Himalayan Zn–Pb–Cu–Ag deposits in the Lanping foreland fold belt, eastern margin of Tibetan Plateau, Ore Geology Reviews (2008), doi:10.1016/j.oregeorev.2008.11.001

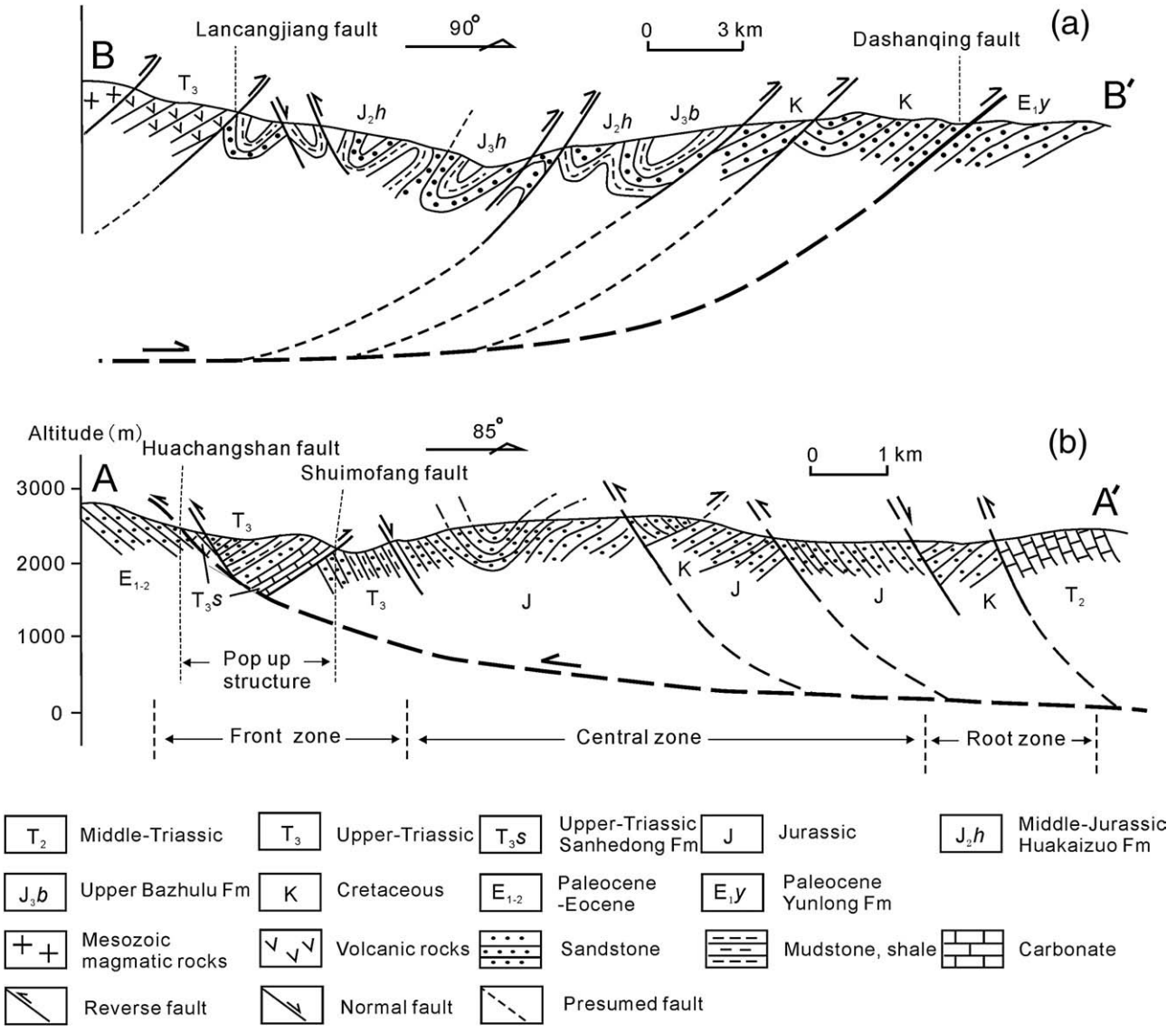

Fig. 5. Geological cross-sections of AA′ and BB′ in the northern Lanping basin, showing the frameworks of (a) the western and (b) the eastern thrust–nappe systems, respectively. See AA′ and BB′ in Fig. 4. Cross-section (b) is modified from He et al. (2004a).

angle thrust faults and steeply-dipping thrust faults in different zones possibly merge into a common east-dipping detachment at depth (Fig. 5b), suggesting that main part of the basinal basement units were overthrust over Tertiary foreland basin.

In the northern segment, the dip angle of E-dipping thrust faults decreases from 60–70° to 30–40° towards the west away from the Huachangshan fault (Fig. 5b). Twinning, lattice deformation, and anomalous extinction of calcite in the clastic rocks of these faults suggest transpressional deformation (He et al., 2004a), whereas the C–T diagram of calcite from the Huachangshan fault indicates that average orientations of σ_1 and σ_3 are NW–SE and NE–SW, respectively, implying thrusting from SE to NW (He et al., 2004a,b).

In the southern segment (Jinding region), the most prominent structural feature is a trap structure in the front zone. It resulted from westward thrusting of the Mesozoic strata over the Tertiary strata along gently-dipping major thrust faults. The overlying Mesozoic strata exhibit a reversed sequence consisting of Upper Triassic (T_3s) and Lower Cretaceous rocks (K_1j), whereas the footwall of the major thrust fault displays a normal sequence dominated by the Eocene Yulonglong Formation (E_1y) and Middle Cretaceous strata (Xue et al., 2007). Numerous thrust faults run parallel to the major thrust fault, and breccias occur in the reversed strata.

4. Distribution of mineral deposits

Over 100 Ag-rich base metallic deposits and occurrences are located in the Lanping basin. Most, including the giant Jinding Zn–Pb, Jiman Cu, Sanshan Zn–Pb–Cu–Ag, and Fulongchang Ag–Cu–Zn–Pb deposits (Table 1), are located in the northern segment of the basin (Hou et al., 2006). Spatially, we classify them into four ore belts, each of which displays distinct structural ore control, host rocks, and bulk metal compositions.

The first belt, called the “Jinman belt”, occurs in the Jurassic intensely folded (root zone) rocks of the western thrust system (Fig. 4). It is generally hosted by red clastics and is controlled by small-scale ~NS-striking faults that were triggered by regional E–W-directional compression and associated thrusting (Fig. 6). The deposits are Cu-dominant, with or without Ag, and include the medium-sized Jinman and Liancheng Cu deposits, and the small Kedengjian (Cu) and Xiaogela (Cu–Ag) deposits (Table 1).

Please cite this article as: He, L., et al., Thrust-controlled, sediment-hosted, Himalayan Zn–Pb–Cu–Ag deposits in the Lanping foreland fold belt, eastern margin of Tibetan Plateau, Ore Geology Reviews (2008), doi:10.1016/j.oregeorev.2008.11.001

Table 1
Geology and features of economically significant deposits in the Lanping foreland fold belt

Name		Metallic comm.	Tonnage	Grade	Structural control	Host rocks	Alteration	Mineral assemblage	Orebody size	Orebody shape	Data source
Jinding		Zn–Pb (–Sr)	Pb 2.64 Mt Zn 12.84 Mt Ag: 1722 t	Pb: 1.16–2.42%, Zn: 8.32–10.52% Ag: 12.5–12.6 g/t	Structural and litholithic trap and dome in the eastern thrust–nappe system	Tertiary limestone-dominated breccias, Cretaceous quartz sandstone	Cal, Do, Si	Gn, Sp, Py, Mc, Cel, Sm	Length: 50–1450 m thickness: 10–102 m depth: 215–1360 m	Strata-like, lenticular, tabular	Liu et al. (1993); Xue et al. (2007)
Baiyangchang		Zn–Pb – Cu–Ag	Under exploration	Ag: 110–245 g/t, Cu: 0.36–1.61%, Pb: 0.22–3.24%, Zn: 1.11%	The front zone in the eastern thrust–nappe system	Jurassic–Cretaceous high-porous limestone and the overlying low-porous carbonaceous argillite	Ba, Ca	Te, Cp, Bo, Fre, Py, Ar, Sp, Gn, S	Length: 150–405 m thickness: 2.7–17.7 m	Large vein, strata-like, banded	Ye et al. (1992)
Sanshan	Xiaquwu – Dongzhiyan block	Cu–Ag	Zn+Pb: >0.5 Mt Ag: >3000 t Cu: ~0.3 Mt	Ag: 165–189 g/t Pb: no data Zn: no data Cu: 0.38–1.59 %	Fractural zones within hanging-wall and footwall of Huachangshan thrust fault; The front zone in the eastern thrust–nappe system	Upper Triassic dolomitic limestone and breccia limestone; Tertiary sandstone and conglomerate	Do, Cal	Tet, Ar, Py, Az	Length: 320–3494 m thickness: 2.7–8.5 m	Strata-like, sheet-like	Chen et al. (2000)
	Yanzidong block	Cu–Ag – Zn–Pb		Ag: 165–189 g/t Pb: 1.95 % (av.) Zn: 2.41% (av.) Cu:1.11–1.81%	Fractural zones within hanging-wall and footwall of Huachangshan thrust fault; The front zone in the eastern thrust–nappe system	Upper Triassic dolomitic limestone and breccia limestone; Tertiary sandstone and conglomerate	Do, Si, Cal	Cp, Tet, Gn, Sp, Py	Length: 590–2920 m thickness: 2.2–15.2 m	Strata-like, sheet-like	Chen et al. (2000)
	Huachangs-han block	Zn–Pb – Ag		Ag: 15.8 g/t (av.) Pb: 1.46% (av.) Zn: 1.60% (av.)	Fractural zones within hanging-wall and footwall of Huachangshan thrust fault; The front zone in the eastern thrust–nappe system	Upper Triassic dolomitic limestone and breccia limestone	Si, Cal, Flu	Sp, Gn	Length: 135 m thickness: 0.9 m (av.)	Strata-like lenticular	Chen et al. (2000)
	Huishan block	Pb–Zn – Ag		Ag: 114.9 g/t Pb:3.55% Zn: 2.36%	Fractural zones within hanging-wall and footwall of Huachangshan thrust fault; The front zone in the eastern thrust–nappe system	Upper Triassic dolomitic limestone and breccia limestone	Si, Cal, Flu	Sp, Gn	Length: 460 m thickness: 16.9 m (av.)	Strata-like lenticular	Chen et al. (2000)
	Heishan block	Zn–Pb – Ag		Ag: 23.3 g/t (av.) Pb: 1.27% (av.) Zn: 3.39% (av.)	Fractural zones within hanging-wall and footwall of Huachangshan thrust fault; The front zone in the eastern thrust–nappe system	Upper Triassic dolomitic limestone and breccia limestone	Si, Cal, Flu	Sp, Gn	Length: 242 m thickness:5.4 m (av.)	Strata-like lenticular	Chen et al. (2000)
Fulongchang	Fulongchang block	Cu–Ag – Pb–Zn	Ag: ~2000 t Cu: 0.1.2 Mt	Ag: 328–547 g/t Pb: 4.2–7.4% Zn: no data Cu: 0.63–11.70%	NE-striking second-order fault related to a NS-striking thrust fault; the front zone in the western thrust–nappe system	Lower–Cretaceous quartz sandstone, siltstone, and mudstone, partially hosted by Middle–Jurassic mudstone	Si, Ca	Tet, Py, Cp, Gn, Fre	Length: 85–882 m thickness: 1.3–2.4 m depth: >100 m	Large veins, lenticular	Chen (2006)
	Baiyangping block	Cu–Ag–Co		Ag: 3.0–33.8 g/t Pb: no data Zn: no data Cu: 0.86–3.3% Co: 0.10–0.27%	NE-striking second-order fault related to a NS-striking thrust fault; the front zone in the western thrust–nappe system	Lower–Cretaceous quartz sandstone and siltstone	Si, Ser, Ca, Epi	Tet, Py, Cp, Gn, Fre	Length: 510–2090 m thickness: 1.9–4.3 m	Large veins, vein	Chen (2006) Zhao (2006)
Wudichang		Zn–Pb – Ag	Under exploration	Ag: 89–255 g/t Pb: 4.2–10.4% Zn: 12.2–15.33% Cu: no data	~EW-striking strike-slip fault	Jurassic mudstone, sandstone, and carbonates	Cal, Si, Arg	Sp, Gn	Length: 600–1126 m thickness: 2.6–3.4 m depth: >80 m	Vein, lenticular	Chen (2006)
Hetaoping		Cu–Ag	Under exploration	Ag: 51 g/t Pb: no data Zn: no data Cu: 0.9–2.1%	~EW-striking strike-slip fault	Cretaceous quartz sandstone, siltstone, and mudstone	Cal, Si, Arg	Tet, Bo, Cp, Gn	Length: 100–1300 m thickness:0.8–2.7 m	Vein	Chen (2006) Zhao (2006)
Jinman (and Liancheng)		Cu	Cu: 0.2 Mt Under exploration	Cu: 0.65–12.0%	NNE-striking compressive fault; the root zone of the western thrust–nappe system	Middle–Jurassic feldspathic quartz sandstone, mudstone, carbonaceous shale, and slate	Ca, Si	Tet, Cp, Bo, Cc, Py	Main veinlet: length: 1350 m thickness: 8.1 m depth: 350 m Network orebodies: length: 35 m thickness: 0.7–17.3 m	Large vein	Zhao (2006)

Alteration abbreviations. Arg: argillization, Ba: baritization, Cal: calcitization, Ca: carbonatization, Do: dolomitization, Epi: epidotization, Flu: fluoritization, Ser: sericitization, Si: silicification.
Ore mineral abbreviations. Ar: argentite, Az: azurite, Bo: bornite, Cc: chalcocite, Cel: celestite, Cp: 7chalcopyrite, Fre: freibergite, Gn: galena, Mc: marcasite, Py: pyrite, Sm: smithsonite, Sp: sphalerite, Tet: tetrahedrite.

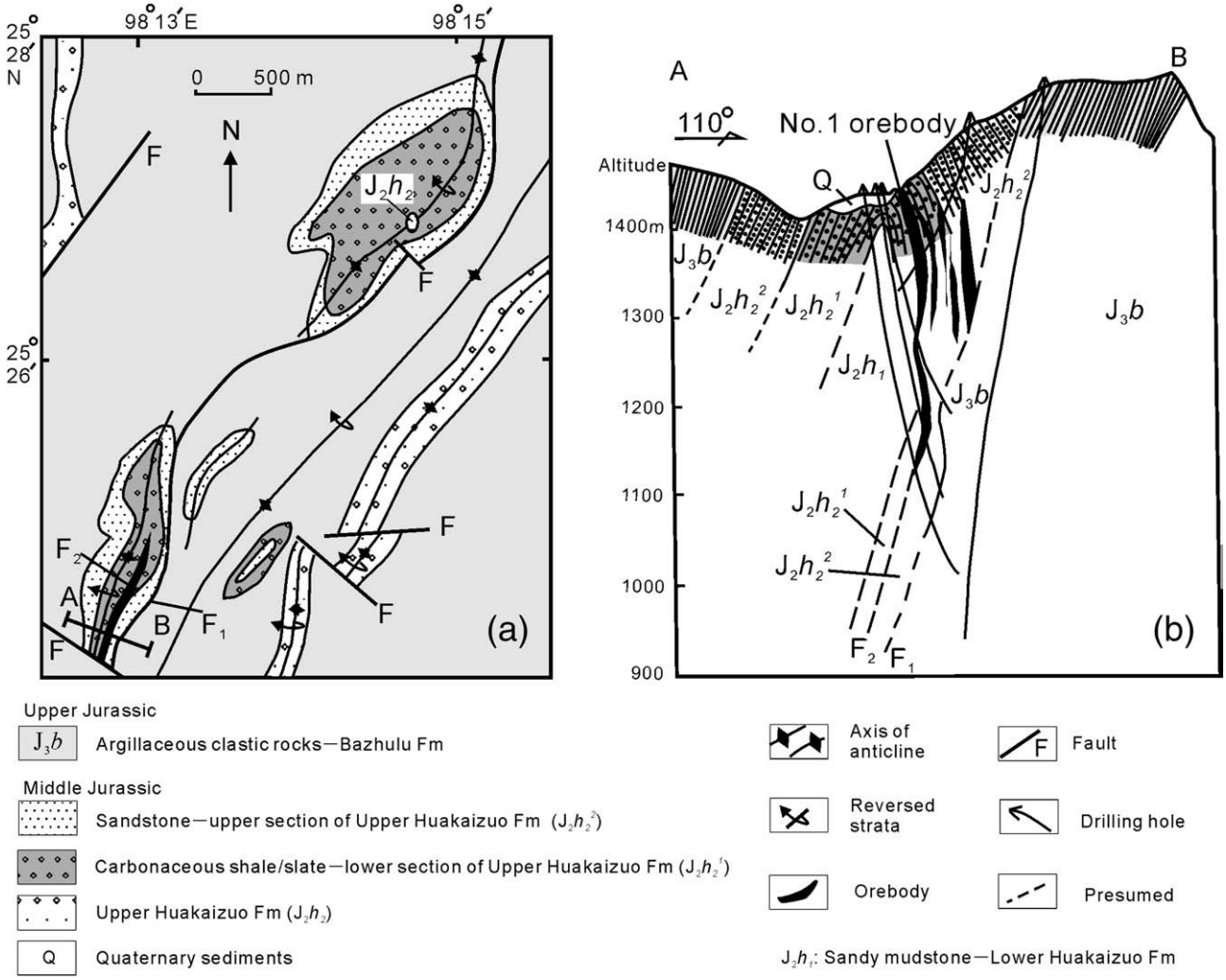

Fig. 6. (a) Simplified geologic map of the Jinman deposit, after Ji and Li (1998) and (b) a cross-section through the orebody (modified from Gao et al., 2006).

The second belt, the "Fulongchang belt", appears in the front zone of the western thrust system. It is Cu–Ag-dominant and locally rich in Pb, Zn, and Co. Deposits include the Fulongchang (Baiyangping) Cu–Ag–Pb–Zn deposit, Hetaoqing Cu–Ag deposit and Wudichang Zn–Pb–Ag deposit (Table 1; Fig. 4). The Fulongchang deposit occurs in NE-striking second-order faults induced by the Sishiliqing thrust fault (Figs. 4 and 7), whereas the Wudichang and Hetaoqing deposits are closely related to ~EW-striking strike-slip faults (Fig. 4). Their host rocks are Jurassic and Cretaceous clastics and marls.

The third belt is located in the front zone of the eastern thrust system. The deposits are related to the Huachangshan thrust fault and the associated back thrust fault (Shuimofang fault) (Fig. 4). The belt is ca. 25 km long and consists of a series of ore blocks, including the Heishan, Huishan and Huachangshan Zn–Pb–Ag blocks, Yanzidong Cu–Ag–Zn–Pb block, Xiaquwu Cu–Ag (–Pb–Zn–Cu) block, Dongzhiyan Ag–Cu(–Sr) block, and Hexi Sr(–Pb) block (Fig. 8). The belt is generally rich in Zn, Pb, Ag, Cu, and Sr; richer in Zn and Pb in the south and richer in Ag, Cu, and Sr in the north. Host rocks are dominated by Triassic carbonates for the Pb–Zn-rich orebodies and, locally, Tertiary clastics for the Cu-rich orebodies.

The fourth ore belt is located in the front zone of the eastern thrust system where the gently NS-striking F_2 thrust fault and associated trap structure control the distribution of the orebodies. The belt is Zn–Pb-dominated and represented by the giant Jinding Zn–Pb(–Sr) deposit.

5. Geology of main deposits

5.1. Jinman Cu deposit

The Jinman deposit contains >0.2 Mt Cu metal, grading 0.30 to 12.02% Cu, and occurs in Jurassic reversed strata of the western thrust–nappe system. The following description is mainly summarized from previous studies (Ji and Li, 1998; Liu et al., 2001; Xu et al., 2004; Wang et al., 2005; Gao et al., 2006; Zhao, 2006).

The deposit is controlled by a NNE-striking compressive fault F_2 (Fig. 6a) that was probably induced by regional eastward thrusting. The fault is developed on the eastern limb of the Jinman reverse anticline, and generally dips to NWW at 60 to 90°, although dipping locally to SEE (Fig. 6a, b). It was formed between sandstone and carbonaceous shale/slate of the Middle Jurassic Upper Huakaizuo Formation (J_2h_2), but, downwards, also cuts the lower Huakaizuo Formation (J_2h_1) (Fig. 6b). Regionally, alongside the Jinman reverse anticline, there are also a series of ~NS- or NE-striking reversed folds. All are developed on the eastern limb of the NS-striking Enqi anticlinorium (Fig. 6a). These folds are cut by the EW- or NW-striking strike-slip faults where no mineralization is found (Gao et al., 2006).

Dependent on the F_2 fault, the deposit mainly occurs in the J_2h_2 strata and locally in the J_2h_1 strata (Fig. 6b). The J_2h strata are composed of terrestrial-marine facies clastic rocks interbedded carbonates. The rocks suffered low-grade metamorphism and some

Please cite this article as: He, L., et al., Thrust-controlled, sediment-hosted, Himalayan Zn–Pb–Cu–Ag deposits in the Lanping foreland fold belt, eastern margin of Tibetan Plateau, Ore Geology Reviews (2008), doi:10.1016/j.oregeorev.2008.11.001

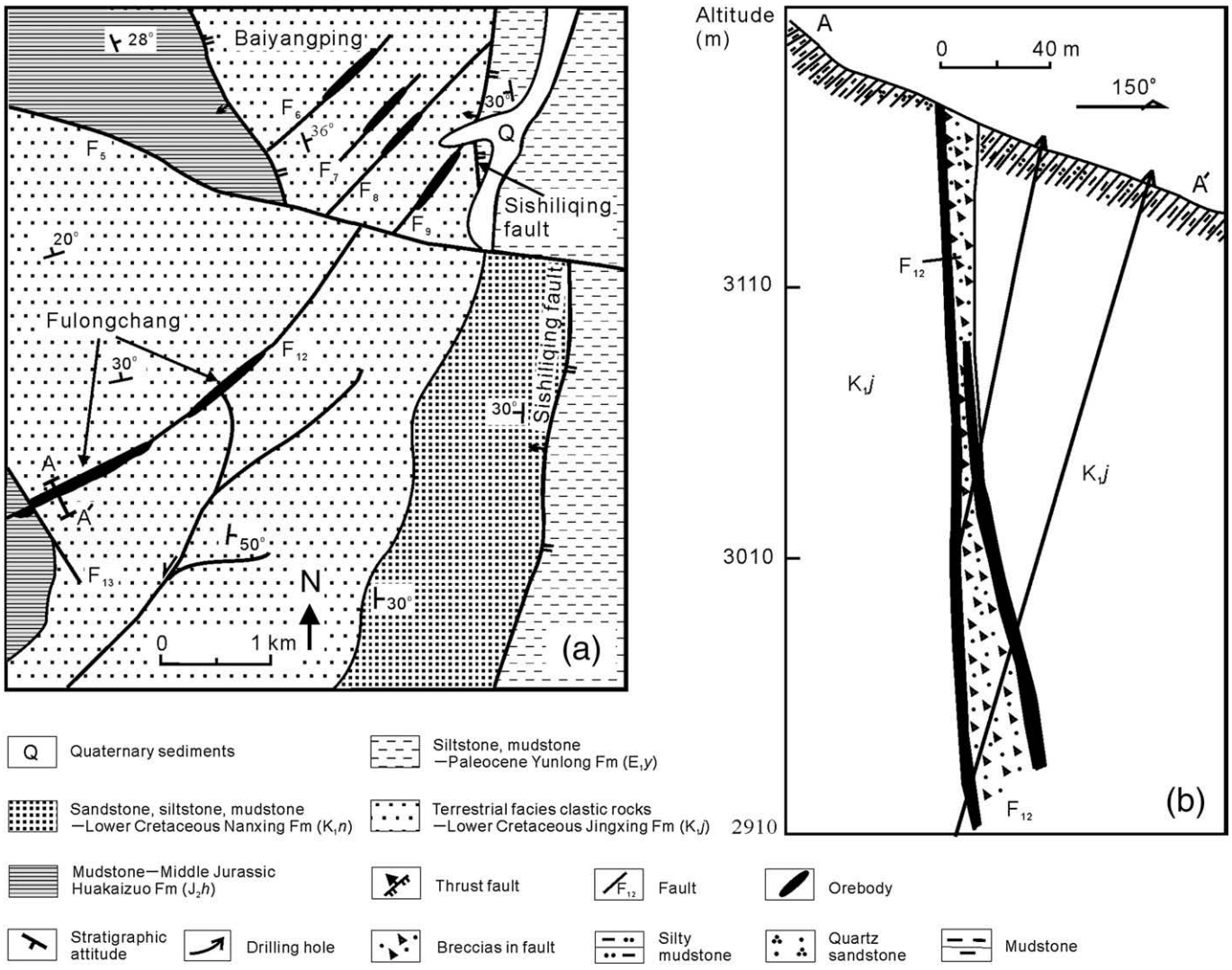

Fig. 7. (a) Simplified geologic map of the Fulongchang-Baiyangping deposit and (b) a cross-section through the orebody of the Fulongchang deposit (modified from Tian, 1997).

were metamorphosed into schist and slate. Close to the orebody, the host rocks are feldspathic quartz sandstone, mudstone, carbonaceous shale and slate. They underwent weak silicification and carbonatization to form siliceous rocks, quartz, calcite, dolomite, and siderite, but no alteration halo can be outlined. Besides the J_2h strata, the Upper Jurassic Bazhulu Formation (J_3b) occurs in the area as red terrestrial-facies argillaceous clastic rocks interbedded with sandstone in which no deposits occur (Fig. 6b).

The main No. 1 orebody is a large vein concordant with the F_2 fault (Fig. 6b). Minor network orebodies occur in fault-bound fractures within feldspathic quartz sandstone of the $J_2h_2^2$ strata. The No.1 orebody is 1350 m long and 1.2 to 15 m wide, and downward extends for 350 m, grading 0.65 to 12.02% Cu (Zhao, 2006). Copper-bearing sulfides include tetrahedrite, arsenian tetrahedrite, Ag-bearing tetrahedrite, chalcopyrite, bornite and chalcocite (Gao et al., 2006). Other sulfides identified are pyrite, pyrrhotite, sphalerite and galena. Gangue minerals are dominated by quartz, with minor calcite, ankerite, barite, siderite, sericite, chlorite, rare bitumen and graphite (Zhao, 2006). The ores are predominantly of vein and stockwork types, with minor massive ores showing characteristics of open-space filling. Locally, the ores are banded and stratiform, indicating that syndiagenetic-sedimentary mineralization is possibly present (Liu et al., 2001).

Cross-cutting and paragenetic relationships allow identification of three mineralization stages. From early- to late-stage, the mineral assemblages are: (1) quartz+pyrite+chalcopyrite+arsenopyrite, with minor bornite, tetrahedrite, and calcite, (2) quartz+pyrite+chalcopyrite+bornite+tetrahedrite+covellite+sphalerite+calcite+minor arsenopyrite, (3) quartz+chalcopyrite+bornite+tetrahedrite+covellite+sphalerite+calcite+minor pyrite and chalcocite (Xu et al., 2004; Zhao, 2006).

5.2. Fulongchang Zn–Pb–Ag–Cu deposit

The Fulongchang deposit, consisting of two blocks, the Fulongchang and Baiyangping blocks, has traditionally been called the "western ore zone of the Baiyangping district" by local geologists. It contains ~2000 t Ag, 0.12 Mt Cu and minor reserves of Zn and Pb (Table 1).

At the scale of the ore zone, there are three groups of faults, including the N–S-striking Sishiliqing thrust fault and its second-order NE-striking faults, F_6–F_9, F_{12}, and the ~EW strike-slip fault F_5 that offsets these two groups (Fig. 7a). Fault F_{12} strikes more than 3 km, and mainly occurs in Cretaceous, locally in Jurassic strata (in the south of the ore zone). The Fulongchang block occurs in the second-order fault F_{12} that generally dips to SE at 60° to 90° and has an extensional–torsional character. The Baiyangping block is, in contrast, hosted by the second-order faults F_6–F_9 (Fig. 7b).

The Fulongchang deposit appears, spatially from NE to SW, in the Lower Cretaceous Jingxing Formation (K_1j) and in the Middle Jurassic Huakaizuo Formation (J_2h). Orebodies are mainly hosted by K_1j quartz

Please cite this article as: He, L., et al., Thrust-controlled, sediment-hosted, Himalayan Zn–Pb–Cu–Ag deposits in the Lanping foreland fold belt, eastern margin of Tibetan Plateau, Ore Geology Reviews (2008), doi:10.1016/j.oregeorev.2008.11.001

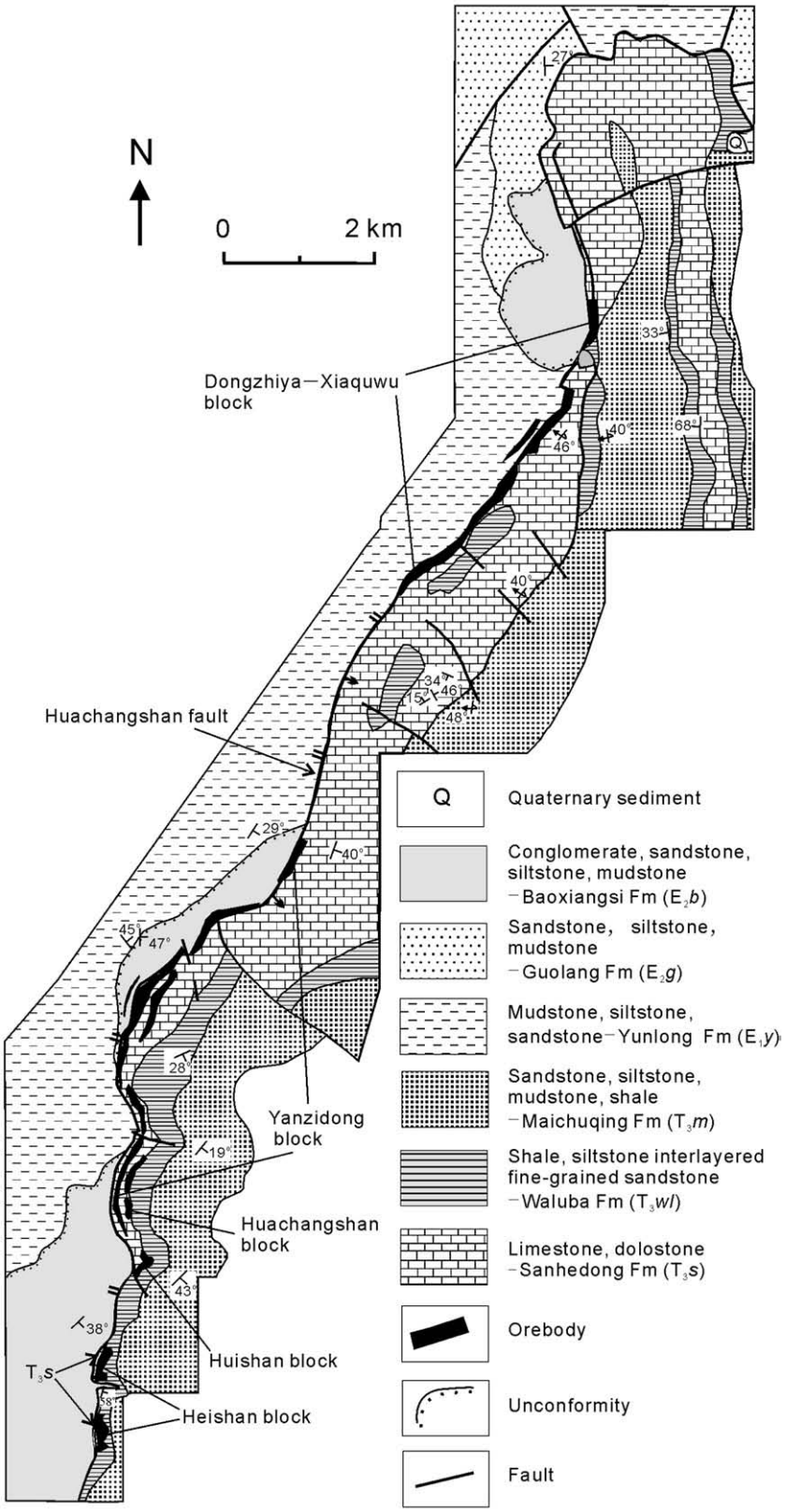

Fig. 8. Simplified geologic map of the Sanshan deposit.

sandstone, siltstone, and mudstone, and partially by J_2h siliceous mudstone. Due to faulting, cracked rocks and fault gouge were formed; these consequently became the host rocks (Fig. 7b). Alteration of the host sequences is commonly present as carbonization and baritization. Minor amounts of pyritization and silicification can also be found.

The orebodies at Fulongchang occur as veins and lenses concordant with the F_{12} fault (Fig. 7a, b). Zinc is especially enriched in the

Please cite this article as: He, L., et al., Thrust-controlled, sediment-hosted, Himalayan Zn–Pb–Cu–Ag deposits in the Lanping foreland fold belt, eastern margin of Tibetan Plateau, Ore Geology Reviews (2008), doi:10.1016/j.oregeorev.2008.11.001

orebody. Sphalerite-dominant veins and cementation breccias are common, but grades and reserves are less well defined. Lead is locally enriched and attains a grade of 7.4% (Zhao, 2006). Primary ores are of vein, breccia-cement, network, and minor massive types. Ore minerals include sphalerite, galena, tetrahedrite, arsenian tetrahedrite, argentite, and Hg-bearing native silver, and coexist with sulfides such as pyrite and chalcopyrite. Cu is mainly present in tetrahedrite, which occurs as euhedral–anhedral grains, commonly coexisting with chalcopyrite (Zhao, 2006). Silver is present as Hg-bearing native silver ('*kongsbergite*'), with minor amounts in tetrahedrite and argentite (Zhao, 2006). Sulfides in the primary ores are commonly subhedral–anhedral in morphology. Mineralization is dominated by open-space filling and cementation. Gangue minerals include calcite, siderite, barite, and quartz (Chen et al., 2000). Based on mineral crosscutting and paragenetic relationships, calcite veining occurred in the early stage and calcite cements belong to the latest stage; sulfides were deposited between these two stages.

5.3. The Sanshan Zn–Pb–Ag–Cu deposit

The Sanshan Zn–Pb–Ag–Cu deposit, traditionally referred to as the eastern ore zone of the Baiyangping district, is the second largest deposit in the Lanping basin. It contains reserves >0.5 Mt Zn+Pb, >3000 t Ag, and ~0.3 Mt Cu, with grades from 1.6% to 3.3% Zn, 0.81% to

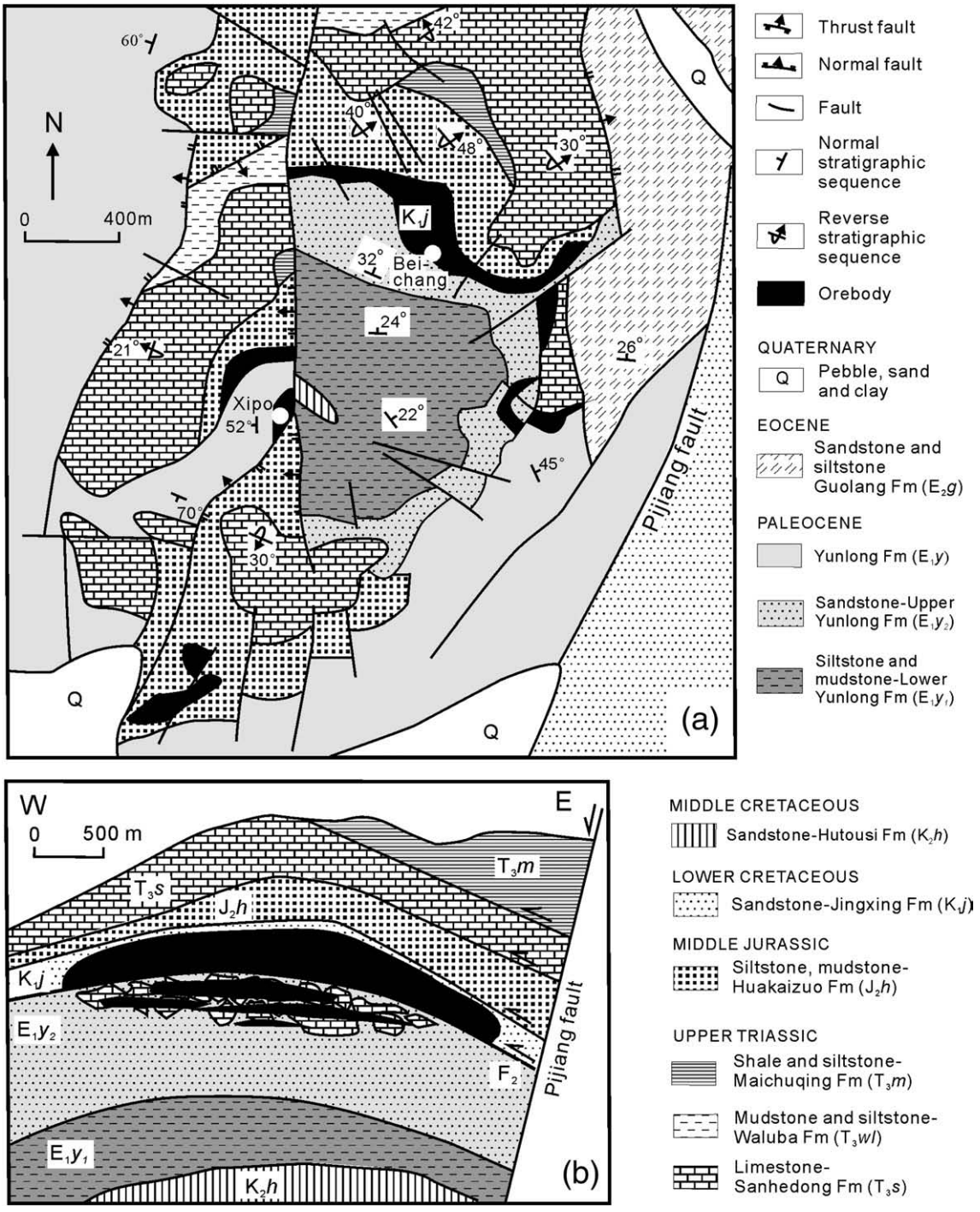

Fig. 9. (a) Geologic map of the Jinding Zn–Pb deposit (after Geological Exploration Report of Jinding Zn–Pb Deposit, Third Geological Surveying Party of Yunnan Geological and Mineral Resources Bureau, 1984), and (b) an sketch cross-section through the orebody in EW direction (modified from Xue et al., 2007).

Please cite this article as: He, L., et al., Thrust-controlled, sediment-hosted, Himalayan Zn–Pb–Cu–Ag deposits in the Lanping foreland fold belt, eastern margin of Tibetan Plateau, Ore Geology Reviews (2008), doi:10.1016/j.oregeorev.2008.11.001

3.55% Pb, and 23.3 to 220.1 g/t Ag. The deposit consists of several ore blocks, mainly distributed along the Huachangsan thrust fault (Fig. 8).

The Sanshan deposit is located in the front zone of the eastern thrust system, controlled by the Huachangshan thrust fault (Fig. 8). The Huachangshan fault generally dips to east, but shows local, reversed dipping in the Dongzhiyan-Xiawuqu block. The fractured zone is 10 to 20 m wide, and shows lithologic zoning varying from an inner compressional schistose zone to an outer crack rock zone. Most ore blocks occur in the fault and crack rock zones within the hanging-wall carbonate sequences (T_3s), but some orebodies of the Yangzidong and Dongzhiya-Xiaquwu blocks are located in the footwall strata, i.e., the Tertiary sandstones (E_1y, E_1b) (Fig. 8). In addition, within the whole ore district, mineralization also occurs in the Kaduo and Sandajie areas (see Fig. 8), which are controlled by the Shuimofang back thrust fault (Fig. 4). Approximately E–W-striking strike-slip faults in the eastern thrust system usually cut these orebodies off, indicating that the faults postdate mineralization.

The host sequence to the Sanshan deposit consists of carbonates of the Upper-Triassic Sanhedong Formation (T_3s) and underlying sandstones of Paleocene Yulong (E_1y) and Eocene Baoxiangsi

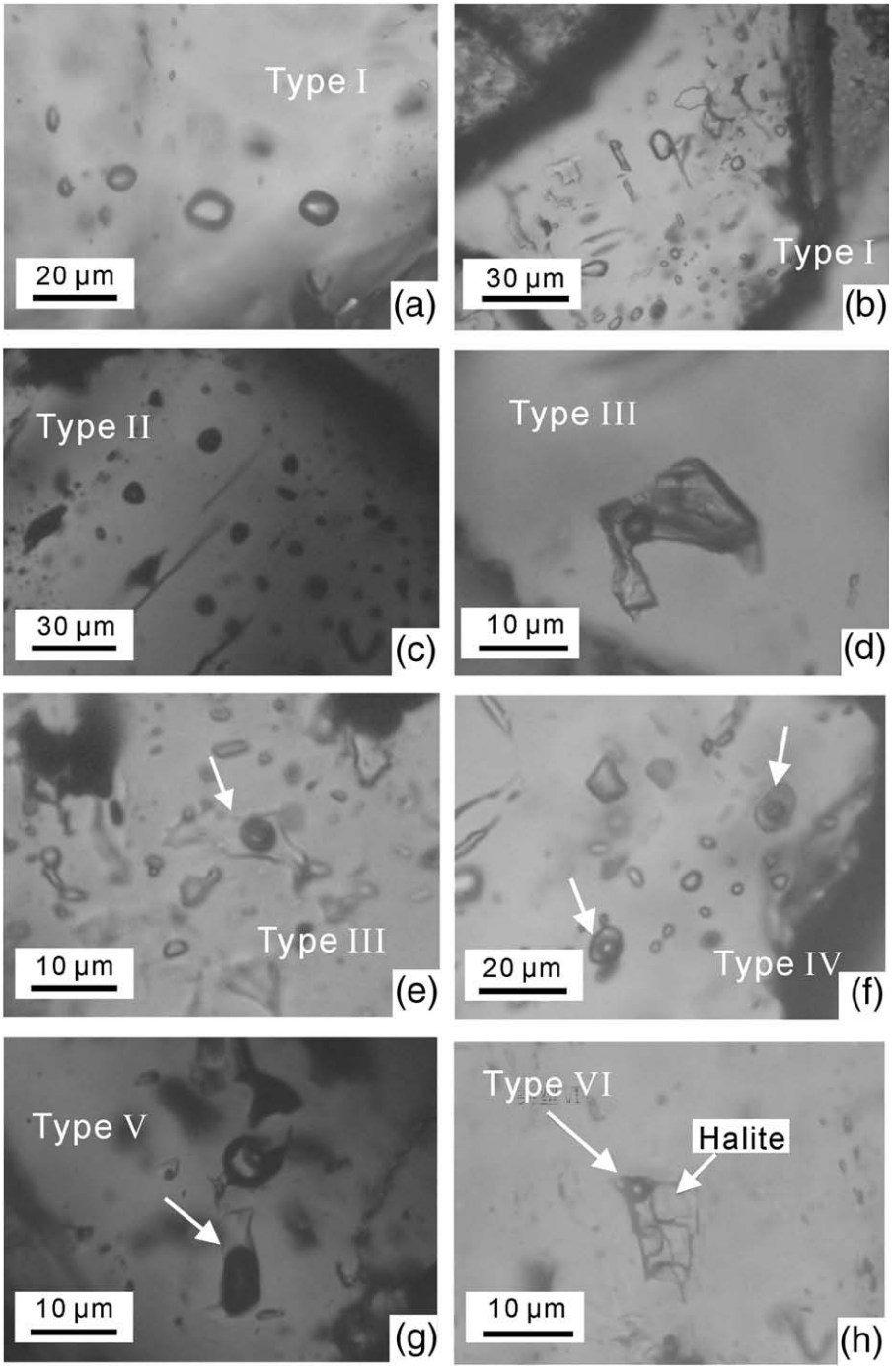

Fig. 10. Fluid inclusion types from the Zn–Pb–Cu–Ag deposits in the Lanping basin. (a) and (b) Single-phase H_2O inclusions in celestite and barite from Dashanjie block of the Sanshan deposit and Dapingzi deposit in Fulongchang ore belt, respectively. (c) Vapor CO_2 inclusions in sphalerite from Kaduo block of the Sanshan deposit. (d) and (e) two-phase H_2O inclusion in calcite and celestite from Xiaquwu block of the Sanshan deposit and Dasanjie block of the Sanshan deposit, respectively. (f) H_2O–CO_2 inclusions in quartz from Huishan block in the Sanshan deposit. (g) A hydrocarbon-rich inclusion in celestite from Dongzhiya block of the Sanshan deposit. (h) H_2O inclusion containing salt daughter mineral in siderite from Hetaoqing deposit in the Fulongchang belt. Note: "H_2O" termed above does not mean pure water but denotes an aqueous solution with certain salinity.

Please cite this article as: He, L., et al., Thrust-controlled, sediment-hosted, Himalayan Zn–Pb–Cu–Ag deposits in the Lanping foreland fold belt, eastern margin of Tibetan Plateau, Ore Geology Reviews (2008), doi:10.1016/j.oregeorev.2008.11.001

Table 2
Homogenization temperature and salinity of fluid inclusions from ore deposits in the Lanping basin

Sample	Min.	T_h (°C)	Sal. (wt.%)	Sample	Min.	T_h (°C)	Sal. (wt.%)	Sample	Min.	T_h (°C)	Sal. (wt.%)
Jianman ore belt											
After Ji and Li, 1998				After Xu and Li, 2003				After Xu and Li, 2003			
Refer to Fig.11[a]				s01133[a]	Quartz?	165	7.0	s01142[c]	Quartz	190	9.6
After Xu and Li, 2003				s797117[b]	Quartz	195	8.3	s01152[c]	Quartz	177	9.2
ss97085 [a]	Quartz	193	9.9	s797118[b]	Quartz	137	3.2	s01144[c]	Quartz	202	8.7
Fulongchang ore belt											
After Xu and Li, 2003				After Chen et al., 2004				After Chen et al., 2004			
s01071[g]	Quartz	283	n.d.	H78[d]	Calcite	147	7.4	H127[f]	Barite	182	14.9
ss97065[e]	Quartz	166	n.d.		Calcite	157	7.7		Barite	190	23.5
ss97066[e]	Quartz	189	5.3		Quartz	97	18.8		Barite	218	16.6
ss97072[d]	Calcite	137	6.1		Quartz	102	17.9	H160[g]	Quartz	122	16.1
ss97076[d]	Quartz	142	n.d.		Quartz	116	21.8		Quartz	146	20.6
ss97078[d]	Quartz	141	6.3		Quartz	117	21.8	H162[g]	Siderite	145	19.7
ss97081[d]	Calcite	132	n.d.		Quartz	131	21.9		Siderite	154	20.5
s01188 [h]	Calcite	174	n.d.		Calcite	144	21.7		Siderite	165	17.9
s01203 [i]	Quartz	182	n.d.	H84[e]	Quartz	132	20.7	XTIL[h]	Calcite	114	18.9
After Chen et al., 2004					Calcite	122	21.0		Calcite	120	n.d.
H74[d]	Calcite	138	26.1	H85[e]	Quartz	106	20.2	XTIL[h]	Calcite	121	18.9
	Calcite	131	27.1		Calcite	125	20.3		Barite	190	18.1
	Quartz	92	27.7		Quartz	162	21.4		Barite	219	23.5
	Calcite	145	24.9		Calcite	130	21.6		Barite	170	15.5
	Calcite	142	25.3		Calcite	156	21.5		Barite	182	15.7
H76 [d]	Quartz	127	22.9		Calcite	130	19.0		Barite	158	15.5
	Calcite	133	25.0		Quartz	151	16.3		Barite	209	10.3
	Quartz	125	22.5	H123 [e]	Quartz	154	16.5		Barite	213	10.3
	Calcite	142	25.3		Quartz	155	17.5		Barite	220	10.3
H78 [d]	Quartz	146	17.1		Quartz	167	15.5		Barite	224	10.3
	Quartz	117	16.0		Quartz	127	15.6		Barite	240	10.4
	Quartz	121	22.2		Quartz	130	18.3		Barite	224	10.5
	Calcite	124	7.3	H127 [f]	Barite	154	20.2	CK9B [h]	Calcite	117	6.3
	Calcite	117	17.6		Barite	156	21.2		Calcite	133	5.8
	Calcite	134	25.0		Barite	171	21.2		Calcite	115	6.6
	Calcite	124	25.0		Barite	160	14.3		Calcite	133	6.5
	Calcite	127	25.0		Barite	220	14.5		Calcite	132	7.2
	Calcite	137	7.3		Barite	210	13.8		Calcite	140	6.9
	Calcite	143	7.4		Barite	153	14.7				
Sanshan ore deposit											
After Xu and Li, 2003				After Chen et al., 2004				After Chen et al., 2004			
ss97037	Calcite	152	n.d.	H95	Quartz	162	17.0	H17	Celestite	136	6.6
ss97038	Calcite	160	3.0		Quartz	184	17.0		Celestite	138	7.8
ss97039	Quartz	147	4.2		Quartz	135	17.1		Celestite	185	9.0
ss97054	Quartz	158	n.d.		Quartz	145	17.0		Celestite	164	9.1
ss97054	Quartz	205	n.d.	H10	Celestite	165	7.3	H138	Sphal.	128	20.4
ss97057	Quartz	158	n.d.		Celestite	171	7.4		Sphal.	133	19.0
ss97012	Calcite	162	n.d.		Celestite	179	7.6		Sphal.	142	19.4
s01170	Quartz	157	5.2		Celestite	141	7.2		Sphal.	152	19.9
ss97049	Calcite	229	6.4		Celestite	144	7.2		Sphal.	115	19.9
After Chen et al., 2004		Celestite	145	7.3		Celestite	152	9.1			
H91	Quartz	204	3.4		Celestite	160	7.1	H138	Sphal.	144	10.0
	Quartz	205	4.2	H17	Celestite	182	7.1		Sphal.	146	10.0
	Quartz	239	4.2		Celestite	191	7.5		Sphal.	150	10.3
	Calcite	116	5.7		Celestite	113	7.6		Sphal.	128	18.8
	Calcite	123	6.5		Celestite	120	7.6		Sphal.	155	10.3
	Calcite	132	6.4		Celestite	106	7.6		Sphal.	163	10.4
	Calcite	143	6.4		Celestite	110	6.8		Sphal.	152	14.8
	Quartz	152	7.2		Celestite	128	8.1		Sphal.	161	15.4
	Calcite	114	6.0		Celestite	131	7.3		Sphal.	170	15.2
H95	Quartz	151	16.5								
Jinding ore deposit											
After Xue et al., 2007				After Xue et al., 2007				After Xue et al., 2007			
Pmp05-6	Quartz	189	n.d.		Gypsum	112	2.8		Calcite	135	4.0
	Quartz	181	9.8	Xp00-9	Sphal.	133	4.1		Calcite	135	1.8
	Celestite	181	9.1		Celestite	106	14.5	$Bch_2$06	Celestite	120	1.6
Pmp20-1	Sphal.	234	9.5	Xp01-2	Calcite	129	4.3		Celestite	119	3.6
	Sphal.	204	9.9		Calcite	110	4.8		Celestite	146	1.9
	Celestite	170	10.7		Calcite	128	5.9		Celestite	120	n.d.
	Celestite	133	4.8		Calcite	114	5.6		Celestite	115	n.d.
Jysh004	Quartz	250	n.d.		Calcite	105	n.d.	Xp-009	Calcite	87	3.6
	Quartz	176	5.6		Calcite	91	n.d.		Calcite	87	3.1
	Quartz	175	n.d.	Xp99-23	Gypsum	92	4.0		Calcite	101	3.6
	Quartz	176	5.9		Gypsum	101	5.3		Calcite	99	4.3
	Quartz	165	n.d.		Gypsum	99	2.8		Calcite	89	n.d.

(continued on next page)

Please cite this article as: He, L., et al., Thrust-controlled, sediment-hosted, Himalayan Zn–Pb–Cu–Ag deposits in the Lanping foreland fold belt, eastern margin of Tibetan Plateau, Ore Geology Reviews (2008), doi:10.1016/j.oregeorev.2008.11.001

Table 2 (*continued*)

Sample	Min.	T_h (°C)	Sal. (wt.%)	Sample	Min.	T_h (°C)	Sal. (wt.%)	Sample	Min.	T_h (°C)	Sal. (wt.%)
After Xue et al., 2007				After Xue et al., 2007				After Xue et al., 2007			
Jysh48-1	Celestite	309	9.1		Gypsum	98	n.d.	Xp56-12	Calcite	87	n.d.
	Celestite	275	4.6	Xp-007	Sphal.	128	16.4		Calcite	77	3.0
	Celestite	262	5.9		Celestite	105	n.d.		Calcite	75	5.5
Jysh8-09	Sphal.	174	13.6	Jysh51-h	Sphal.	126	9.3		Calcite	86	n.d.
	Sphal.	195	5.8		Sphal.	158	13.6	Fxsh55	Sphal.	115	18.0
	Sphal.	196	4.9		Celestite	161	4.3		Celestite	98	14.7
	Sphal.	190	7.8		Celestite	180	3.2	Fzsh102	Calcite	120	6.1
	Celestite	280	8.4		Celestite	174	7.1		Calcite	83	4.4
Jysh37-5	Sphal.	182	5.1		Quartz	166	10.5		Calcite	73	4.9
	Sphal.	194	14.1	Jysh01-9	Calcite	140	4.7		Calcite	70	n.d.
	Sphal.	185	n.d.		Calcite	162	4.7		Calcite	67	n.d.
	Celestite	262	4.3		Calcite	256	3.9		Calcite	59	1.7
Bch006	Sphal.	143	4.1	$Jysh_21$	Gypsum	141	4.0		Calcite	88	3.0
	Celestite	161	4.9		Gypsum	138	3.9		Calcite	85	n.d.
Bch43	Calcite	131	3.2	Bch_25–4	Quartz	157	11.7		Calcite	79	n.d.
	Calcite	135	1.7		Sphal.	190	n.d.	Fzsh01-22	Gypsum	98	4.8
	Calcite	130	3.6		Sphal.	185	9.8		Gypsum	66	2.6
Bch52-5	Gypsum	132	n.d.		Sphal.	175	n.d.		Gypsum	54	5.5
	Gypsum	130	1.6		Celestite	180	6.1				
	Gypsum	116	2.5	Bch60-3	Calcite	240	5.0				

Notes: Min. — Host mineral; Th — Homogenisation temperature; Sal. — Salinity (wt.% NaCl equiv.), n.d.— not determined, Sphal. — Sphalerite. "Refer to Fig. 11" means that the data are shown only on that figure since no number was given in the respective publication. Superscripts a to i represent the names of ore deposits: a — Jinman; b — Xiaogela; c — Kedengjian; d — Fulongchang; e — Baiyangping; f — Dapingzi; g — Hetaoqing; h — Wudichang; i Juputang. Data reported by Ji and Li (1998) and Chen et al. (2004) were derived from a Chaixmeca (−180 to 600 °C) heating–cooling stage at Yichang Institute of Geology and Mineral Resources, with precision better than 0.1 °C (<30 °C) and 2 °C (>3 °C). The data of Xu and Li (2003) were obtained using a LinkamTH600 heating–cooling stage at Chinese University of Geosciences (Wuhan), with precision better than 0.2 °C (<30 °C) and 1–5 °C (>30 °C). The data of Xue et al. (2007) were determined by a LINKAM-TMS94 heating–cooling stage at Chang'an University, with precision better than 0.1 °C (<30 °C) and 1–2 °C (>30 °C).

Formations (E_2b) (Fig. 8). The T_3s carbonates, a significant ore horizon, are composed of thick black to grey, brecciated limestone, dolomitic limestone and dolomite in the lower part and grey, brecciated, siliceous limestone and muddy limestone at upper levels. The upper carbonate sequence hosts orebodies in the Huishan, Heishan, and Huachangshan ore blocks, whereas the lower carbonate sequence hosts orebodies in the other ore blocks. Some orebodies of the Yangzidong block are hosted by E_1b pebbled sandstones. Mineralization also occurs in the E_1y quartz sandstones and mudstones in the Dongzhiya-Xiaquwu block.

Alteration of the host rocks is dominated by dolomitization, calcification, and silicification, but is relatively weak, so that it is difficult to outline a clear alteration halo. Alteration mineral assemblages are simple, and consist of pyrite, barite, fluorite, calcite, celestite, dolomite, and minor quartz.

There are at least 20 orebodies, occurring as veins, lenses, semi-layered and irregular bodies. Individual orebodies vary from 135 to 3500 m in length, 2.3 to 17 m in thickness, and tens up to 320 m in depth. They generally dip to east but locally dip to west along the Huachangshan fault (Fig. 8) (Chen et al., 2004). The ~25 km long ore deposit displays a compositional zoning northwards from Zn–Pb, Zn–Pb–Ag, Cu–Ag, Ag–Cu, to Sr-dominant ores. The dominant ore veins show open-space filling. Ore minerals include sphalerite, galena, pyrite (marcasite) and Cu-sulfides (tetrahedrite, Ag- and As-tetrahedrite, chalcocite, chalcopyrite, and bornite) with minor tenorite, cerussite, smithsonite, azurite, and covellite. Gangue minerals consist of calcite, celestite, siderite, dolomite, barite, fluorite and minor quartz (Chen et al., 2000).

5.4. The Jinding Zn–Pb deposit

The Jinding deposit is the largest Zn–Pb deposit in China with reserves of 200 Mt ore grading 6.08% Zn and 1.29% Pb. Jinding is also the youngest sediment-hosted supergiant Zn–Pb deposit in the world (Xue et al., 2007). The tabular orebodies are hosted in Cretaceous and Tertiary terrestrial siliciclastic rocks. The deposit suffered from intense oxidization due to high relief, forming a thick well-developed oxidized zone that accounts for 40% of the total reserve. This deposit has been studied by many authors (e.g., Shi et al., 1983; Qin and Zhu, 1991; Zhou and Zhou, 1992; Luo et al., 1994; Li and Kyle, 1997; Kyle and Li, 2002; Xue et al., 2007); its geology and mineralization features are briefly described here.

5.4.1. Ore controls

The Zn–Pb mineralization is controlled by the thrust fault F_2 and a structural dome with a diameter of ~3 km formed during late-stage uplift (Fig. 9a, b). The fault F_2 is a major westward-thrusting fault in the region and represents the boundary between "exotic" and *in situ* strata. It can generally be treated as horizontal, but dips outwards at low angles due to late-stage uplifting. The mineralization occurs in its hanging- and footwall. The orebodies are distributed around the core of the dome and dip outwards. Due to numerous radial faults related to doming and mineralization which postdate the normal faults, the ca. 40 m thick orebody was cut into six ore blocks around the core (Fig. 9a). Their thickness increases towards the core and reaches a maximum at the top of the dome.

5.4.2. Host rocks

The host sequences consist of permeable coarse-grained siliciclastics of the Jinxing Formation (K_1j), and pebbled sandstone and limestone breccias of the Upper Yunlong Formation (E_1y_2), blanketed by two impermeable units consisting of mudstone and siltstone sequences of the overlying Huakaizuo Formation (J_2h) and underlying Lower Yunlong Formation (E_1y_1), respectively (Fig. 9b). The K_1j sandstones consist of quartz and siliceous lithic fragments with minor feldspar. Their cements are dominated by calcite with some calcareous clay, which were partially or almost entirely replaced by sulfides, celestite, and minor barite. The E_1y_2 host rocks consist of pebbled sandstones and limestone breccias. There are two types of breccia: ore-rich breccias related to diaper-intrusion of over-pressured ore-forming fluids; and a barren breccia linked to gypsum dissolution and regional thrusting (Wang et al., 2007). Fragments of the ore-enriched breccias are usually poorly-rounded, and dominated by bitumen-bearing limestones with minor sandstone and mudstone. Interstitial materials are fine-grained sandstones with lesser calcareous and argillaceous materials in which sulfide minerals are

Please cite this article as: He, L., et al., Thrust-controlled, sediment-hosted, Himalayan Zn–Pb–Cu–Ag deposits in the Lanping foreland fold belt, eastern margin of Tibetan Plateau, Ore Geology Reviews (2008), doi:10.1016/j.oregeorev.2008.11.001

disseminated. The barren breccias consist of fragmented carbonates, gypsum-rich rocks, mudstone, and siltstone, and the interstitial materials of calcite, siltstone, fine-grained sandstone, gypsum, and anhydrite (Wang et al., 2007).

5.4.3. Mineralization

In the upper ore zone (i.e., in the hanging-wall K_1j sandstone), the orebodies are tabular and stratabound, and the ores show typical replacement features. In the lower ore zone (in the footwall E_1y_2 units), the orebodies are more variable in shape and occur as lenses, veins and bodies of irregular shape (Fig. 9b). The ores are of typical open-space filling and replacement. In general, the 3-dimensional shape of the whole orebody is mushroom-like, with an ore-bearing sandstone cap and ore-bearing breccia root (Xiu et al., 2006), dominated by Zn–Pb ores with variable Zn/Pb ratios from 0.3 to 7.8 (Xue et al., 2007).

More than 30 primary minerals have been identified in the Jinding deposit. Besides dominant sphalerite and galena, there are other sulfides (pyrite, marcasite, chalcopyrite, argentite, and tetrahedrite), sulfates (celestite, anhydrite, gypsum, and barite), carbonates (calcite), quartz, and bitumen of various compositions (Xue et al., 2007). Cross-cutting mineral paragenetic relationships allow three mineralization stages to been recognized: (1) fine-grained disseminated sphalerite + galena + quartz; (2) coarse-grained galena + sphalerite + celestite veins; and (3) coarse-grained galena + calcite + celestite + gypsum as cement.

6. Fluid inclusions

6.1. Inclusion types

On the basis of the phase assemblages at room temperature and their compositions, fluid inclusions in hydrothermal minerals from the ores can be categorized into six types. Type I inclusions are composed of pure liquid aqueous solution (LH_2O) (Fig. 10a, b). Type II inclusions are vapor-rich and composed of H_2O, CO_2, or CH_4 (Fig. 10c). Type III inclusions are composed of liquid aqueous solution and water vapor (LH_2O+VH_2O) (Fig. 10d); type IV inclusions consist of aqueous solution and single- or two-phase CO_2 ($LH_2O+VCO_2\pm LCO_2$) (Fig. 10e, f). Type V are hydrocarbon-rich inclusions that commonly contains H_2O and CO_2 (Fig. 10 g), and Type VI are three-phase H_2O inclusions containing salt daughter minerals ($LH_2O+VH_2O+SNaCl$) (Fig. 10h).

All type inclusions are clustered within the host minerals or are isolated or occur along healed fractures. Among them, type I, type III, and type IV inclusions can be found almost in each deposit. Type IV inclusions are rarer and Type VI is found only in the Fulongchang ore deposit. Type II is rare and secondary. Type V inclusions are also rare and only found in the Dongzhiya and Huishan ore districts of the Sanshan deposit.

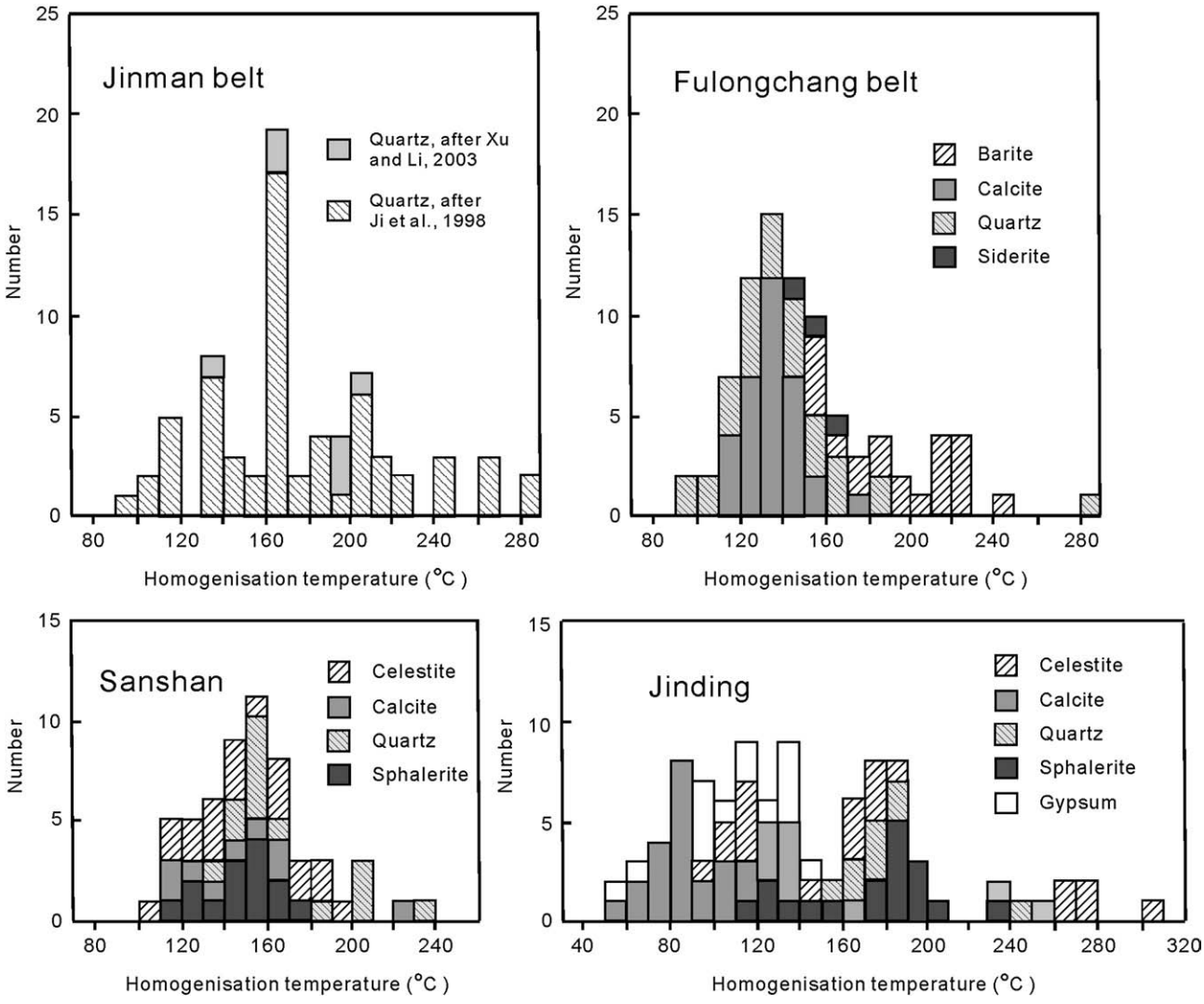

Fig. 11. Histogram of homogenization temperature of fluid inclusions from the ore belts/deposits in the Lanping basin. Data are listed in Table 2.

Please cite this article as: He, L., et al., Thrust-controlled, sediment-hosted, Himalayan Zn–Pb–Cu–Ag deposits in the Lanping foreland fold belt, eastern margin of Tibetan Plateau, Ore Geology Reviews (2008), doi:10.1016/j.oregeorev.2008.11.001

6.2. Homogenisation temperature and salinity

Published homogenization temperatures (T_h) and salinities (Ji and Li, 1998; Xue et al., 2007; Xu and Li, 2003; Chen et al., 2004) were obtained from primary fluid inclusions in sphalerite and other hydrothermal gangue minerals that coexist with galena, Cu-sulfides, and/or sphalerite. In such cases, type III inclusions are dominant with minor type IV and type VI. The paragenetic position of those hydrothermal minerals is not well described in many if the published accounts. To our knowledge, in the Jinman ore belt, host quartz derives from the quartz vein containing Cu-sulfides. The vein, a key ore type, is very distinct from other hydrothermal minerals. In Fulongchang and Sanshan, barite, quartz, and celestite occur in the early-stage mineralization; calcite, sphalerite, and siderite occur in both early- and late-stages. In Jinding, Xue et al. (2007) identified that quartz occurs in the early stage, sphalerite and celestite in the early- and middle-stages, calcite in the middle- and late-stages, and gypsum in the late-stage.

A total of 306 T_h data were obtained, ranging from 54 to 309 °C (mean 155 °C) for all deposits (Table 2). Most values are generally lower than 240 °C (Fig. 11). Divided by deposit, the range is 90 to 290 °C (mean ~177 °C and peak values at 160 to 170 °C) for the Jinman ore belt, 92 to 283 °C (mean 152 °C, peak values at 130 to 140 °C) for the Fulongchang ore belt, 106 to 239 °C (mean 153 °C, peak values at 150 to 160 °C) for the Sanshan deposit, and 54 to 309 °C (mean 143 °C, three peak values at 80 to 100 °C, 100 to 140 °C, and 170 to 190 °C) for the Jinding deposit (Table 2, Fig. 11). The mean T_h values generally display a decrease from the Jinman belt to the Fulongchang and Sanshan belt/deposits, to the Jinding deposit. However, such an interpretation is inconsistent with the variation of the peak values, which does not exhibit a clear trend.

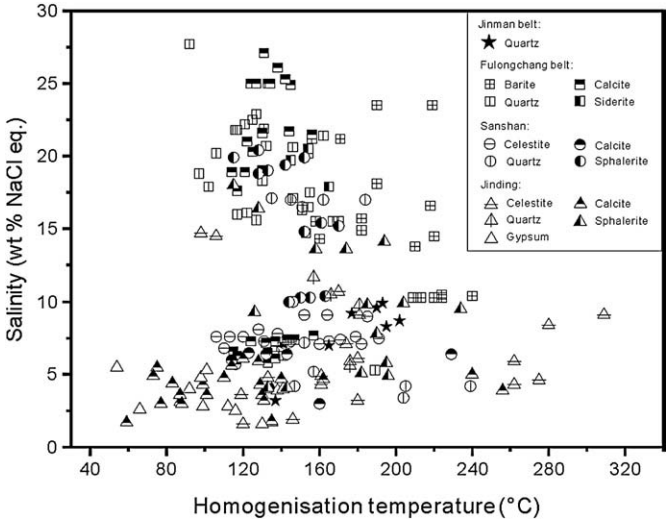

Fig. 13. Plot of homogenization temperature *vs.* salinity of fluid inclusions from the ore belts/deposits in the Lanping basin. Data are listed in Table 2.

Fluid inclusions in sphalerite from the Sanshan and Jinding deposits have homogenization temperatures below 240 °C (Fig. 11). Because they represent credible records of ore-forming fluids, the T_h values may represent actual mineralization temperatures. T_h values in

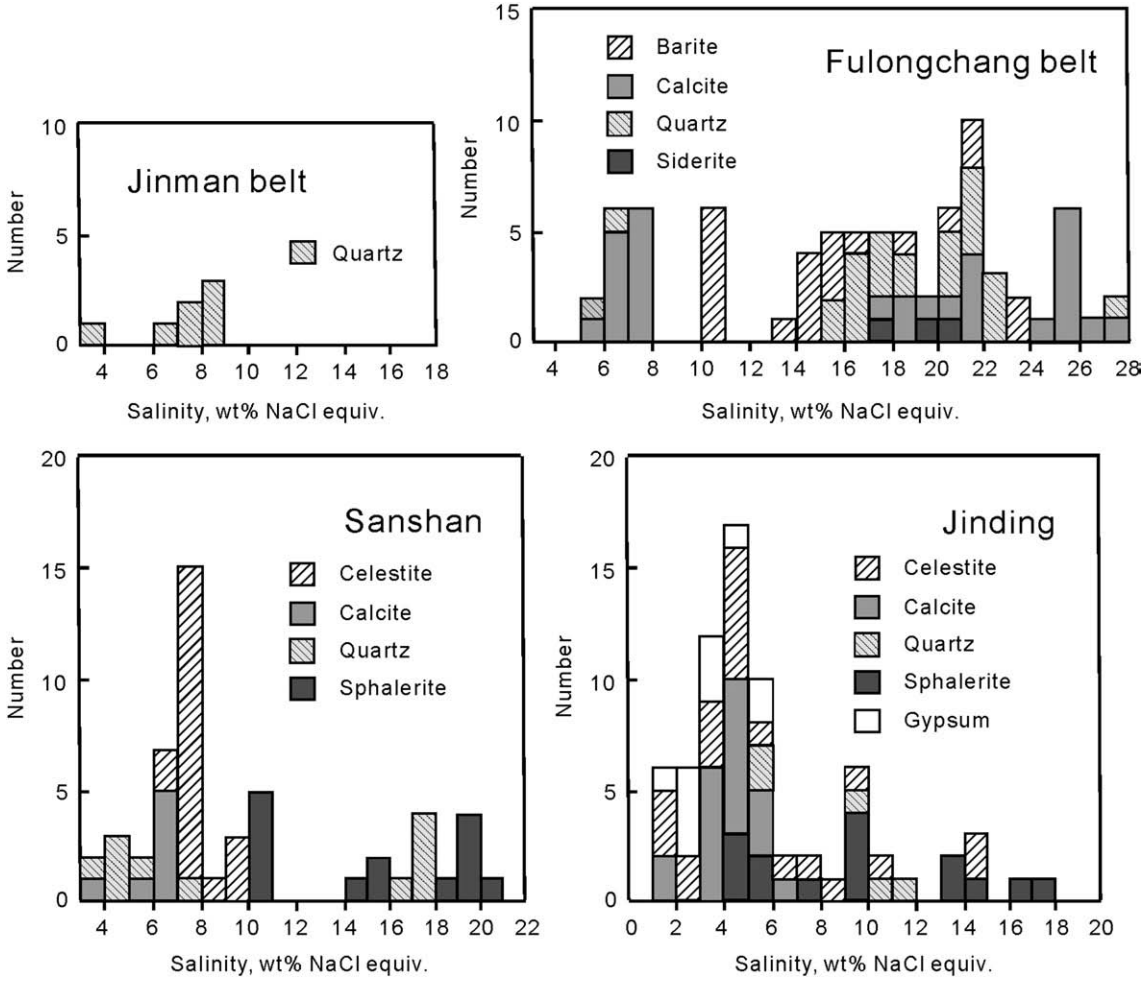

Fig. 12. Histogram of salinity of fluid inclusions from the ore belts/deposits in the Lanping basin. Data are listed in Table 2.

Please cite this article as: He, L., et al., Thrust-controlled, sediment-hosted, Himalayan Zn–Pb–Cu–Ag deposits in the Lanping foreland fold belt, eastern margin of Tibetan Plateau, Ore Geology Reviews (2008), doi:10.1016/j.oregeorev.2008.11.001

Table 3
Lead isotopic compositions of ore sulfides from ore deposits and various rocks in the Lanping basin

Sample	Min.	$^{206}Pb/^{204}Pb$	$^{207}Pb/^{204}Pb$	$^{208}Pb/^{204}Pb$	Sample	Min.	$^{206}Pb/^{204}Pb$	$^{207}Pb/^{204}Pb$	$^{208}Pb/^{204}Pb$
Jinman ore belt									
After Wu et al. (2003)					After Xu and Zhou (2004)				
JM4C [a]	Cpy	18.5866	15.6514	38.7646	①[a]	Tetrah.	18.628	15.581	38.605
JM4T [a]	Tetrah.	18.6481	15.6546	38.8294		Tetrah.	18.639	15.586	38.615
JM23 [a]	Cpy	18.6190	15.6572	38.8022	SS97119 [b]	Tetrah.	18.635	15.675	38.953
JM24 [a]	Tetrah.	18.6407	15.6581	38.8537	S01150 [c]	Tetrah	18.535	15.567	38.766
JM25 [a]	Bornite	18.6580	15.6519	38.8273	After Zhao (2006)				
SX11B [j]	Bornite	18.6582	15.6931	39.0631	JMIII-2 [a]	Chc	18.7031	15.6712	38.9819
SX11T [j]	Tetrah.	18.6545	15.6783	39.019		Bornite	18.6978	15.6748	38.9826
SX36P [j]	Cpy	18.7012	15.6706	38.9950	JMIII-6 [a]	Cpy	18.6846	15.6691	38.8860
SX41T [j]	Tetrah.	18.7379	15.6765	39.0269	JMIII-12 [a]	Cpy	18.6932	15.6707	38.9608
After Xu and Zhou (2004)	TCH1-7 [b]	Chc	18.7015	15.6873	39.0497				
①[a]	Tetrah.	18.559	15.590	38.555	SL1-1 [b]	Chc	18.6753	15.6766	39.0106
					RDH2-3 [l]	Chc	18.7399	15.6802	38.9773
Fulongchang ore belt									
After Wei (2001)					After Xu and Zhou (2004)				
? [e]	Tetrah.	18.612	15.605	38.789	S01109 [n]	Tetrah.	18.656	15.680	39.162
? [d]	Galena	18.686	15.677	39.008	S01129 [o]	Tetrah.	18.587	15.620	38.906
? [g]	Cpy	18.582	15.609	38.792	After Li et al. (2005)				
? [f]	Bornite	18.587	15.620	38.812	BYP116 [e]	Tetrah.	18.644	15.609	38.811
After Wang and He (2003)	FLC147 [d]	Tetrah.	18.642	15.618	38.811				
B4-2 [e]	Tetrah.	18.669	15.661	38.948	FLC161 [d]	Tetrah.	18.644	15.611	38.786
B4-3 [e]	Tetrah.	18.626	15.610	38.787	FLC149 [d]	Sphal.	18.643	15.628	38.811
B4-4 [e]	Tetrah.	18.680	15.709	39.068	FLC160 [d]	Sphal.	18.634	15.604	38.768
After Xu and Zhou (2004)				FLC176 [d]	Sphal.	18.622	15.548	38.514	
SS97060 [e]	Tetrah.	18.747	15.754	39.245	After Li et al. (2005)				
SS97074 [d]	Galena	18.672	15.652	38.927	? [d]	Galena	18.690	15.685	39.018
SS97075 [d]	Galena	18.680	15.663	38.963	? [d]	Galena	18.673	15.655	38.943
S01183 [d]	Tetrah.	18.713	15.705	39.244	After Zhao (2006)				
S01060 [g]	Tetrah.	18.716	15.770	39.325	LZP1-1[k]	Galena	18.6816	15.6831	39.0267
S01103 [m]	Tetrah.	18.575	15.638	38.952		Sphal.	18.6924	15.6848	39.0368
Sanshan ore deposit									
After Wei (2001)					After He et al. (2004a)				
?	Sphal.	18.460	15.598	38.638	HX-48-1	Sphal.	18.582	15.659	38.999
?	Galena	18.462	15.611	38.671	DK-2-2	Sphal.	18.764	15.894	38.474
?	Sphal.	18.702	15.710	39.063	HS-48-2	Tetrah.	18.705	15.727	39.255
?	Sulfide	18.682	15.626	38.769	HX-50	Tetrah.	18.682	15.668	39.179
?	Galena	18.696	15.625	38.772	After Xu and Zhou (2004)				
?	Galena	18.670	15.602	38.707	SS97051	Galena	18.610	15.650	38.882
?	Galena	18.619	15.607	38.701	SS97043	Tetrah.	18.569	15.612	38.710
?	Galena	18.659	15.602	38.748	SS97051	Tetrah.	18.613	15.651	38.880
After He et al. (2004)	S01167	Tetrah.	18.715	15.638	39.075				
HS116	Sphal.	18.777	15.708	39.056	S01045	Tetrah.	18.724	15.662	39.069
HX-1	Pyrite	18.460	15.554	38.619	After Zhao (2006)				
HX-2	Pyrite	18.247	15.571	38.419	HCS1-1	Galena	18.7772	15.6844	38.9879
						Chc	18.7430	15.6828	38.9918
Jinding ore deposit									
After Bai et al. (1985)					After Ye et al. (1992)				
BTW1	Galena	18.444	15.625	38.584	J26	Galena	18.196	15.398	38.164
BTW	Sphal.	18.566	15.627	38.675	J27	Galena	18.299	15.469	38.135
BTW2	Galena	18.394	15.583	38.470	J28	Galena	18.223	15.425	38.099
BTW2	Sphal.	18.543	15.676	39.046	J61	Galena	18.161	15.362	38.101
BTW3	Pyrite	18.413	15.597	38.483	J65	Galena	18.205	15.376	38.007
BTW4	Galena	18.405	15.598	38.462	J66	Galena	18.235	15.401	38.009
BTW5	Galena	18.374	15.504	38.243	J69	Galena	18.286	15.420	38.300
BTW5	Sphal.	18.426	15.684	38.266	J72	Galena	18.184	15.390	38.182
BTW7	Galena	18.443	15.628	38.516	J27	Sphal.	18.326	15.489	38.160
BTW8	Galena	18.405	15.552	38.334	J28	Sphal.	18.285	15.470	38.297
Yn16	Galena	18.267	15.465	38.117	J60	Sphal.	18.232	15.435	38.106
Yn23	Galena	18.266	15.436	38.032	J61	Sphal.	18.217	15.374	38.124
Yn25	Galena	18.238	15.404	37.900	J65	Sphal.	18.400	15.607	38.216
Yn30	Galena	18.321	15.496	38.177	J70	Sphal.	18.315	15.461	38.176
Yn31	Galena	18.347	15.521	38.281	J27	Pyrite	18.351	15.499	38.168
Yn38	Galena	18.371	15.54	38.311	J29	Pyrite	18.345	15.524	38.283
Yn41	Galena	18.289	15.45	37.993	J60	Pyrite	18.402	15.542	38.329
Yn42	Galena	18.35	15.532	38.281	J62	Pyrite	18.262	15.468	38.203
Yn45	Galena	18.351	15.516	38.167	J69	Pyrite	18.354	15.521	38.214
Yn46	Galena	18.310	15.483	38.160	After Zhang et al. (1993)				
Yn55	Galena	18.345	15.513	38.204	82j-2	Galena	18.400	15.612	38.463
Yn59	Galena	18.187	15.390	37.889	82j-5	Galena	18.441	15.632	38.660
Yn61	Galena	18.324	15.495	38.169	82j-7	Galena	18.285	15.491	38.300

(continued on next page)

Please cite this article as: He, L., et al., Thrust-controlled, sediment-hosted, Himalayan Zn–Pb–Cu–Ag deposits in the Lanping foreland fold belt, eastern margin of Tibetan Plateau, Ore Geology Reviews (2008), doi:10.1016/j.oregeorev.2008.11.001

Table 3 (*continued*)

Sample	Min.	$^{206}Pb/^{204}Pb$	$^{207}Pb/^{204}Pb$	$^{208}Pb/^{204}Pb$	Sample	Min.	$^{206}Pb/^{204}Pb$	$^{207}Pb/^{204}Pb$	$^{208}Pb/^{204}Pb$
After Bai et al. (1985)					After Zhang et al. (1993)				
Yn87	Galena	18.332	15.488	38.145	82j-9	Galena	18.303	15.501	38.290
Yn93	Galena	18.320	15.430	38.230	82j-1	Galena	18.420	15.628	38.536
Yn13-1	Galena	18.312	15.473	38.135	82j-18	Galena	18.232	15.476	38.174
Yn16-1	Galena	18.292	15.498	38.215	82j-19	Galena	18.283	15.493	38.295
Yn16-2	Galena	18.213	15.373	37.927	82j-26	Galena	18.321	15.450	38.235
Yn30-1	Galena	18.374	15.267	38.315	82j-27	Galena	18.506	15.640	38.557
Yn30-2	Galena	18.169	15.351	38.103	82j-31	Pyrite	18.558	15.617	38.321
Yn31-1	Galena	18.282	15.452	38.040	83j-33	Pyrite	18.600	15.622	38.359
Yn41-1	Galena	18.401	15.548	38.357	82j-35	Galena	18.493	15.619	38.488
Yn42-1	Galena	18.346	15.526	38.286	Lan38	Galena	18.220	15.430	38.090
Yn46-2	Galena	18.313	15.482	38.157	Lan39	Galena	18.210	15.380	38.010
After Zhou and Zhou (1992)					Lan40	Galena	18.210	15.400	38.050
TY37	Galena	18.283	15.462	38.296	Lan42	Galena	18.170	15.360	38.040
TY38	Galena	18.221	15.422	38.093	Lan43	Galena	18.270	15.410	38.230
TY39	Galena	18.207	15.377	38.007	Lan44	Galena	18.290	15.420	38.300
TY40	Galena	18.214	15.399	38.046	Lan46	Galena	18.220	15.410	38.160
TY41	Galena	18.138	15.352	37.921	After Xiu et al. (2006)				
TY42	Galena	18.160	15.361	38.042	JX17	Galena	18.410	15.620	38.569
TY43	Galena	18.246	15.410	38.225	JX18	Galena	18.425	15.640	38.634
TY44	Galena	18.288	15.421	38.301	JX27	Galena	18.523	15.643	38.623
TY45	Galena	18.286	15.452	38.443	JG30	Galena	18.434	15.626	38.599
TY46	Galena	18.220	15.406	38.155	JG32-1	Galena	18.442	15.639	38.638
Ding1	Galena	18.194	15.395	38.112	JX135	Galena	18.436	15.653	38.677
Ding2	Galena	18.150	15.330	37.961	JX165	Galena	18.436	15.649	38.666
Ding3	Galena	18.522	15.634	38.48	JX251-3	Galena	18.421	15.634	38.616
Ding4	Galena	18.416	15.637	38.639	JX27	Sphal.	18.586	15.709	38.821
Yn-9	Galena	18.390	15.600	38.540	JX251-8	Sphal.	18.458	15.679	38.765
Yn-10	Galena	18.170	15.341	37.802	JX93	Pyrite	18.444	15.658	38.693
Yn-13	Galena	18.311	15.470	38.141	JX304	Pyrite	18.456	15.662	38.714
Yn-26	Galena	18.360	15.580	38.440	After Zhao (2006)				
Yn-26-1	Galena	18.410	15.620	38.560	JDJ1-5	Galena	18.4522	15.6651	38.7107
Yn38-2	Galena	18.280	15.450	38.040	JDJ1-9	Pyrite	18.4541	15.6682	38.7255
Yn41-2	Galena	18.40	15.550	38.360	PMP1-2	Galena	18.4404	15.6641	38.7031
Yn42-2	Galena	18.350	15.530	38.290	PMP1-1	Galena	18.4373	15.6625	38.6956

Rocks in the Lanping basin (Xue et al., 2007)

Sample	Strata	Rocks	$^{206}Pb/^{204}Pb$	$^{207}Pb/^{204}Pb$	$^{208}Pb/^{204}Pb$
JB308	Huakaizuo Formation (Middle Jurassic)	Siltstone	18.592	15.742	39.306
JB439	Yunlong Formation (Paleocene)	Sandstone	18.488	15.636	38.632
JB453-1	Yunlong Formation (Paleocene)	Sandstone	18.549	15.693	38.809
No. 1	Jingxing Formation (Lower Cretaceous)	Sandstone	18.517	15.705	38.888
No. 2	Jingxing Formation (Lower Cretaceous)	Sandstone	18.707	15.891	39.317
No. 3	Sanhedong Formation (Upper Triassic)	Limestone	18.544	15.765	38.914
No. 5	Sanhedong Formation (Upper Triassic)	Limestone	18.888	15.988	39.464
Crustal lead of the Lanping basin			18.140–20.289	15.274–16.051	37.878–40.800
Mafic, ultramafic and alkaline rocks in the Lanping basin			17.877–18.353	15.465–15.523	37.797–38.414

Notes: Min. — Host mineral. Cpy — Chalcopyrite; Sphal. — Sphalerite; Tetrah. — Tetrahedrite; Chc — Chalcocite. Superscripts a to o represent the names of ore deposits: a to i are as same as in Table 2; j — Shuixie; k — Liziping; l — Rendianhe; m — Baila; n — Guideng; o — Huangtuqing. The data of Wu et al. (2003) were obtained using an ion thermal ionization mass spectrometer (Finnigan Triton TI) at State Key Laboratory for Mineral Deposits Research, Nanjing University, with the precision better than 0.05%. The data of Xu and Zhou (2004) were determined by a MAT261 mass spectrometer at Open Laboratory for Constitution, Interaction and Dynamics of the Crust–mantle System, Ministry of Land and Resources, with the precision better than 0.1%. The data of Wei and Li (2001) and Wang and He (2003) were determined by a MAT261 mass spectrometer at Yichang Institute of Geology and Mineral Resources, with the precision better than 0.1%. The data of Li et al. (2005), Zhao (2006), He et al. (2004b), andYe et al. (1992) were obtained using a MAT261 mass spectrometer at Laboratory for Isotopic Geology, CAGS, with the precision better than 0.1%. The data of Xiu et al. (2006) were determined by MAT262 at Laboratory for Radiogenic Isotope Geochemistry, Institute of Geology and Geophysics, CAS, with the precision better than 0.11%. In general, chemical treatment of the samples for Pb isotopic analyses in those different laboratories are similar. Samples were washed in distilled water, and digested in a mixture of double distilled concentrated HNO_3 and HCl. Pb was separated and purified by HBr and anion exchange resin, and then coated on a rhenium strip by classic H_3PO_4 and silicon gel method for mass spectrometer analysis. Bai et al. (1985) and Zhou and Zhou (1992) do not give methodology in their publications — it is therefore difficult to evaluate the precision.

early-stage minerals (barite, quartz, celestite) are generally higher (Fig. 11). In Jinding, average T_h values are 182 °C (quartz), 154 °C (sphalerite), 140 °C (celestite), 126 °C (calcite) and 98 °C (gypsum) (Xue et al., 2007). This suggests that temperatures decreased from the early- to late-stage mineralization.

A total of 210 salinity data were determined from deposits in the Lanping basin, varying from 1.6 to 27.7 wt.% NaCl equiv. (mean 11.1 wt.% NaCl equiv.) (Table 2). Divided by deposit, values are 3.2 to 9.9 wt.% NaCl equiv. (mean 8.0) in the Jinman ore belt, 5.3 to 27.7 wt.% NaCl equiv. (mean 16.9) in the Fulongchang ore belt, 3.0 to 20.4 wt.% NaCl equiv. (mean 10.0) in the Sanshan deposit, and 1.6 to 18.0 wt.% NaCl equiv. (mean 6.1) in the Jinding deposit. Histograms (Fig. 12) show that the salinities in the Fulongchang ore belt, Sanshan and Jinding deposits show a bimodal distribution: <11.0 and >13.0 wt.% NaCl equiv. Due to limited data, it is unclear whether such a distribution might also exist in the Jinman ore belt.

Fluid inclusions in sphalerite have higher salinities than those in the other minerals in the Sanshan deposit, but this is not reflected by the data from Jinding (Fig. 12). Temporally, the variation of the salinities is ambiguous; early-stage and other minerals have large fluctuation in the histograms (Fig. 12).

The salinity *vs.* T_h diagram for the total dataset gives two distinct correlation trends (Fig. 13). An approximate negative correlation exists for low-temperature and high-salinity inclusions, whereas a positive

Please cite this article as: He, L., et al., Thrust-controlled, sediment-hosted, Himalayan Zn–Pb–Cu–Ag deposits in the Lanping foreland fold belt, eastern margin of Tibetan Plateau, Ore Geology Reviews (2008), doi:10.1016/j.oregeorev.2008.11.001

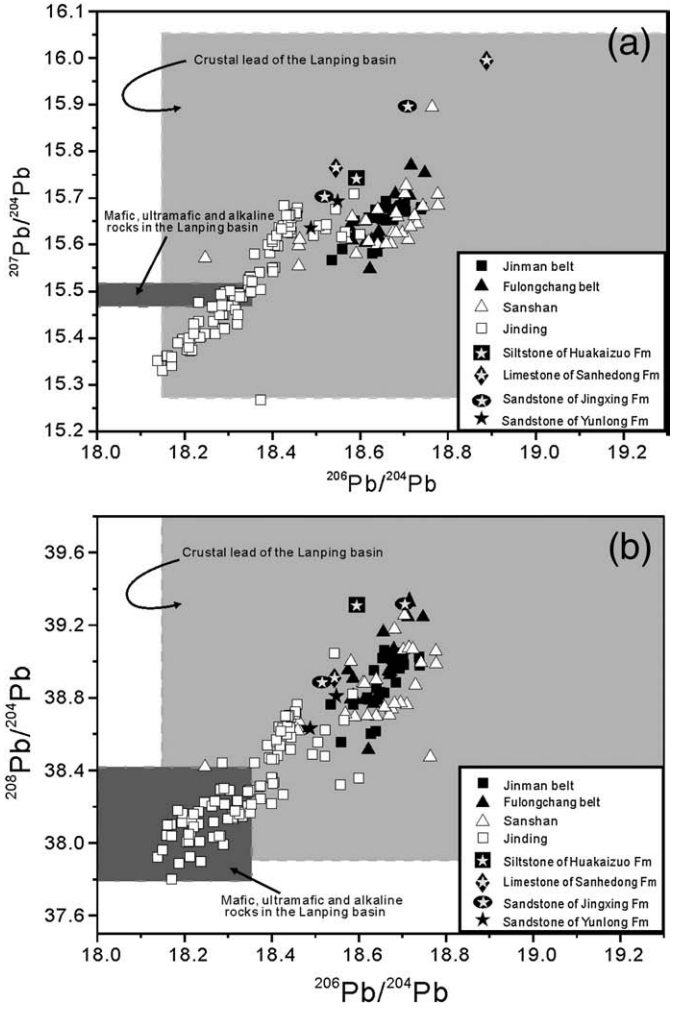

Fig. 14. Plots of (a) $^{207}Pb/^{204}Pb$ *vs.* $^{206}Pb/^{204}Pb$ and (b) $^{208}Pb/^{204}Pb$ *vs.* $^{206}Pb/^{204}Pb$ of ore sulfides from the ore belts/deposits in the Lanping basin. Data are listed in Table 3.

correlation is seen for low-temperature and low-salinity inclusions. Fluid inclusions in the early- and middle-stage minerals in the Fulongchang and Sanshan usually show the negative correlation, whereas those in the Jinding exhibit an approximate positive correlation (Fig. 13).

7. Isotope data

7.1. Lead isotopes

Table 3 lists published lead isotopic data of ore sulfides from deposits in the Lanping basin (Bai et al., 1985; Ye et al., 1992; Zhou and Zhou, 1992; Zhang, 1993; Wei, 2001; Wang and He, 2003; Wu et al., 2003; He et al., 2004b; Xu et al., 2004; Li et al., 2005; Xiu et al., 2006; Zhao, 2006). In total, $^{206}Pb/^{204}Pb$ varies from 18.138 to 18.777 (mean 18.460), $^{207}Pb/^{204}Pb$ is between 15.267 and 15.894 (mean 15.567), and $^{208}Pb/^{204}Pb$ is between 37.802 and 39.325 (mean 38.544). Sub-divided by belt/deposit, the $^{206}Pb/^{204}Pb$, $^{207}Pb/^{204}Pb$ and $^{208}Pb/^{204}Pb$ data are, respectively, 18.535 to 18.740 (mean 18.657), 15.567 to 15.693 (mean 15.653), 38.555 to 39.063 (mean 38.882) in the Jinaman ore belt, 18.545 to 18.747 (mean 18.654), 15.548 to 15.770 (15.652), and 38.514 to 39.325 (mean 38.938) in the Fulongchang ore belt, 18.247 to 18.777 (mean 18.633), 15.554 to 15.894 (mean 15.652), and 38.419 to 39.255 (38.848) in the Sanshan deposit, and 18.136 to 18.600 (mean 18.336), 15.267 to 15.709 (mean 15.511), and 37.802 to 39.046 (mean 38.306) in the Jinding deposit.

Plots of $^{207}Pb/^{204}Pb$ *vs.* $^{206}Pb/^{204}Pb$ and $^{208}Pb/^{204}Pb$ *vs.* $^{206}Pb/^{204}Pb$ (Fig. 14a, b) show that the lead isotopic compositions generally lie in the field of crustal rocks of the Lanping basin and partly overlap the field of upper mantle rocks of the basin. The Jinding deposit differs, however, from the other deposits in that its Pb isotopes are closer to those of upper mantle rocks, whereas the Pb isotopes of the other ore belts/deposit are closer to the sedimentary rocks in the Lanping basin.

7.2. Sulfur isotopes

The 172 published sulfur isotopic data for sulfides from ore deposits in the Lanping basin are shown in Table 4 (Xiao, 1989: Li et al., 1997; Ji and Li, 1998; Liu et al., 2001; Wang and He, 2003; Wu et al., 2003; He et al., 2004b; Li et al., 2005; Zhao, 2006). For all deposits, $\delta^{34}S_{CDT}$ values show a wide range from −30.4 to 11.2‰ (mean −6.2‰). Values are from −20.5 to 7.0‰ (mean −2.5‰) for the Jinman ore belt, from −5.6 to 11.2‰ (mean 6.2‰) for the Fulongchang ore belt, from −7.3 to 10.1‰ (mean −0.5‰) for the Sanshan deposit, and from −30.4 to −1.7‰ (mean −12.7‰) for the Jinding deposit, respectively. The peaks of $\delta^{34}S_{CDT}$ values differ between each ore belt/deposit. They occur at −6 to 2‰ in Jinman, 6 to 8‰ in Fulongchang, −4 to −2‰ in Sanshan, and −20 to −12‰ and −6 to −2‰ in Jinding (Fig. 15). The Fulongchang ore belt clearly has relatively heavier sulfur isotope composition; the Jinding deposit has the lightest sulfur.

7.3. Hydrogen and oxygen isotopes

A total of 49 hydrogen and 50 oxygen isotopic data of water from fluid inclusions in hydrothermal quartz and calcite from the ores are summarized in Table 5 and Fig. 16. All these data are taken from previous publications (Li et al., 1995; Ji and Li 1998; Gong et al., 2000; Liu et al., 2000; Chen et al., 2004; Li et al., 2004; Zhao, 2006). Data from fluid inclusions in sulfides and sulfates have been eliminated because the analytical technique is less reliable. Consequently, no data are given for the Jinding deposit, and only three data are given for the Sanshan deposit.

Table 5 shows that the population of δD_{H2O} (SMOW) values varies from −136 to −30‰ (mean −91‰), and all $\delta^{18}O_{H2O}$ (SMOW) values are between −14.8‰ and 10.0‰ (mean −0.3‰). The Jinamn, Fulongchang, and Sanshan ore belts/deposit have δD values of −136‰ to −30‰ (mean −89‰), −109‰ to −76‰ (mean −94‰), and −122‰ to −78‰ (mean −96‰), respectively. Corresponding $\delta^{18}O$ values are −10.6‰ to 9.8‰ (mean 2.7‰), −14.8‰ to 10.0‰ (mean −8.0‰), and −10.9‰ to −0.6‰ (mean −4.3‰) for Jinamn, Fulongchang, and Sanshan, respectively.

Those data show a wide distribution in the δD–$\delta^{18}O$ diagram (Fig. 16), but fall predominately in the field between the meteoric water line (MWL) and the fields below metamorphic and primary magmatic waters. A few data occur in the fields of metamorphic and primary magmatic waters. It can be seen that the δD values have a relative stable range between −120‰ and −70‰, whereas the $\delta^{18}O$ values are strongly variable, from −15‰ to 10‰.

7.4. Carbon and oxygen isotopes

A total of 79 carbon and 81 oxygen isotopic measurements of hydrothermal calcite, dolomite, siderite, and strontianite from the ores are shown in Table 6 and Fig. 17. These data are compiled from previous studies (Yan, 1993; Luo et al., 1994; Li et al., 1995; Chen et al., 2000; Gong et al., 2000; Xue et al., 2002; Liu et al., 2001; Xu and Li, 2003; Liu et al., 2004; Li et al., 2004; Li et al., 2005; Zhao, 2006). Table 6 shows that the total $\delta^{13}C$ (PDB) values change from −24.5 to 2.7‰ (mean 1.6‰), with −7.4 to −4.8‰ (mean −5.4‰) for the Jinman ore belt, −4.2 to 2.3‰ (mean −2.2‰) for the Fulongchang ore belt, −8.3 to 2.7‰ (mean −2.2‰) for the Sanshan deposit, and −24.5 to −6.1‰ (mean −18.6‰) for the Jinding deposit, respectively. The range of $\delta^{18}O$ (SMOW) values is between −2.5 and 24.3‰ (mean 12.9‰): 4.2 to

Please cite this article as: He, L., et al., Thrust-controlled, sediment-hosted, Himalayan Zn–Pb–Cu–Ag deposits in the Lanping foreland fold belt, eastern margin of Tibetan Plateau, Ore Geology Reviews (2008), doi:10.1016/j.oregeorev.2008.11.001

Table 4
Sulfur isotopic compositions of ore sulfides from ore deposits in the Lanping basin

Sample	Min.	$\delta^{34}S$, CDT ‰	Sample	Min.	$\delta^{34}S$, CDT ‰	Sample	Min.	$\delta^{34}S$, CDT‰
Jianman ore belt								
After Xiao (1989)			After Ji and Li (1998)			After Liu et al. (2001)		
1 [a]	Cpy	−20.46	Jm-35 [a]	Bornite	−2.47	S-7 [a]	Cpy	−5.55
Jiangxi-3 [a]	Cpy	−1.34	Jm-9 [a]	Bornite	−9.32	S-12 [a]	Tetrah.	−4.28
?	Cpy	−5.86	After Liu et al. (2001)			JM-2 [a]	Bornite	2.55
Jiangdong-1 [a]	Tetrah.	−0.08	Jm-8 [a]	Pyrite	5.70	S-4 [a]	Bornite	−1.34
Jiangxi-1 [a]	Tetrah.	−4.57	Jd-1 [a]	Cpy	−0.32	After Wu et al. (2003)		
2 [a]	Tetrah.	1.40	Jx-3 [a]	Cpy	−0.86	JM-4 [a]	Cpy	−10.2
Jiangdong-2 [a]	Bornite	−9.08	Lk-2 [a]	Cpy	0.63	JM-23 [a]	Cpy	−15.5
3 [a]	Bornite	−9.75	Tc11-1 [a]	Cpy	−3.81	JM-4 [a]	Tetrah.	3.2
Jiangxi-2 [a]	Bornite	−5.49	By-1 [a]	Tetrah.	4.18	JM-12 [a]	Tetrah.	1.1
After Li et al. (1997)			Jd-2 [a]	Tetrah.	1.98	SX-36[j]	Tetrah.	0.7
S5-2-3 [j]	Tetrah.	−0.07	Tc4-1 [a]	Tetrah.	1.68		Cpy	4.2
S5-2-4 [j]	Tetrah.	−0.05	Lk5-1 [a]	Tetrah.	−1.09		Tetrah.	1.8
After Ji et al. (1998)			Jx-1 [a]	Tetrah.	3.31	SX-41 [j]	Tetrah.	1.9
Jm-10 [a]	Cpy	−8.86	Jx-2 [a]	Bornite	−3.15	After Zhao (2006)		
	Cpy	−3.88	Jd-3 [a]	Bornite	2.07	JMIII-6 [a]	Cpy	−4.8
Jm-15 [a]	Cpy	−0.52	Lk5-2 [a]	Bornite	−2.95	JMIII-12 [a]	Cpy	−7.2
Jm-19 [a]	Pyrite	−5.83	S-12 [a]	Cpy	−5.06	JMIII-2 [a]	Bornite	−7.2
Jm-3 [a]	Cpy	−0.51	S-2 [a]	Cpy	−5.67		Chalcocite	−7.6
Jm-6 [a]	Cpy	−1.57	S-3 [a]	Cpy	1.26			
Jm-1 [a]	Tetrah.	7.00	S-4 [a]	Cpy	0.54			
Fulongchang ore belt								
After Wei (2001)			After Wang and He (2003)			After Li et al. (2005)		
? [d]	Galena	5.03	B4-2 [e]	Tetrah.	6.71	FLC149 [d]	Sphal.	10.5
? [e]	Tetrah.	6.10	B4-3 [e]	Tetrah.	6.79	FLC-160 [d]	Sphal.	10.0
? [f]	Bornite	5.84	B4-4 [e]	Tetrah.	6.91	FLC-176 [d]	Sphal.	11.2
? [g]	Cpy	2.51		Tetrah.	6.83	BY-3-1 [e]	Tetrah.	5.8
? [d]	Galena	2.54		Tetrah.	6.10	BY-3-2 [e]	Tetrah.	9.3
? [d]	Galena	−5.64	After Li et al. (2005)			BYP116 [e]	Tetrah.	9.1
			FLC-147 [d]	Tetrah.	9.2	H-1 [d]	Tetrah.	3.5
			FLC161[d]	Tetrah.	7.9	H-2 [d]	Tetrah.	4.8
Sanshan ore deposit								
After Wei (2001)			After He et al. (2004)			After Zhao (2006)		
?	Sphal.	−1.24	DK-2-1	Pyrite	−0.1	DK-2-2	Sphal.	2.1
?	Sphal.	−4.14	HX-1	Pyrite	10.1	HX-48-1	Sphal.	2.0
?	Galena	−3.54	HX-2	Pyrite	10.1	HX-48-2	Tetrah.	1.8
?	Galena	−3.97				DK-1	Tetrah.	−2.9
?	Galena	−7.33				DK-50	Tetrah.	−3.2
?	Galena	−3.89						
?	Galena	−3.67						
Jinding ore deposit								
After Zhou and Zhou (1992)			After Zhou and Zhou (1992)			After Zhou and Zhou (1992)		
Ty1	Galena	−2.96	Ty53	Pyrite	−13.32	24	Galena	−5.97
Ty2	Mar.	−21.43	Ty55	Galena	−18.46	25	Galena	−5.36
Ty3	Mar.	−19.47	Ty57	Galena	−12.04	31	Galena	−3.83
Ty4	Sphal.	−14.59	Ty58	Sphal.	−13.00	After Ye et al. (1992)		
Ty5	Pyrite	−19.13	Ty59	Pyrite	−11.55	J26	Pyrite	−13.60
Ty6	Galena	−2.69	Ty60	Galena	−24.91	J26	Sphal.	−14.62
Ty8	Galena	−14.86	Ty64	Pyrite	−15.21	J26	Galena	−19.90
Ty9	Mar.	−20.36	Ty65	Pyrite	−16.10	J27	Pyrite	−13.90
Ty10	Pyrite	−3.84	BTW1	Galena	−18.43	J27	Sphal.	−15.91
Ty11	Galena	−22.68	BTW1	Pyrite	−14.89	J27	Galena	−18.91
Ty12	Mar.	−12.37	BTW2	Pyrite	−18.82	J28	Sphal.	−15.15
Ty13	Galena	−2.60	BTW2	Galena	−17.28	J28	Galena	−20.60
Ty14	Sphal.	−1.71	BTW3	Sphal.	−15.21	J29	Pyrite	−15.30
Ty15	Galena	−20.50	BTW3	Sphal.	−15.11	J60	Pyrite	−3.87
Ty15	Mar.	−13.79	BTW4	Galena	−19.80	J60	Sphal.	−4.20
Ty16	Galena	−22.68	BTW5	Galena	−9.70	J61	Sphal.	−3.92
Ty17	Galena	−13.26	BTW5	Sphal.	−10.58	J61	Galena	−5.63
Ty18	Galena	−20.54	BTW8	Galena	−23.56	J62	Pyrite	−5.68
Ty20	Galena	−12.20	JZK400-1	Pyrite	−15.49	J63	Pyrite	−3.36
Ty21	Galena	−30.43	JZK400-2	Pyrite	−16.80	J65	Pyrite	−3.99
Ty22	Galena	−5.40	JZK402-1	Pyrite	−15.37	J65	Sphal.	−4.81
Ty23	Galena	−10.50	JZK402-2	Pyrite	−13.48	J65	Galena	−5.92
Ty24	Galena	−6.00	1TS2	Galena	−14.80	J66	Pyrite	−3.45
Ty25	Sphal.	−7.67	1TG1	Galena	−18.40	J66	Galena	−5.10
Ty26	Pyrite	−13.88	1TG3	Galena	−17.70	J69	Pyrite	−4.01
Ty27	Galena	−16.81	Yn93	Galena	−24.94	J69	Galena	−4.79
Ty29	Galena	−6.60	22	Galena	−5.44	J70	Sphal.	−7.00
Ty32	Galena	−7.57	23	Galena	−10.50	J72	Galena	−19.30

Please cite this article as: He, L., et al., Thrust-controlled, sediment-hosted, Himalayan Zn–Pb–Cu–Ag deposits in the Lanping foreland fold belt, eastern margin of Tibetan Plateau, Ore Geology Reviews (2008), doi:10.1016/j.oregeorev.2008.11.001

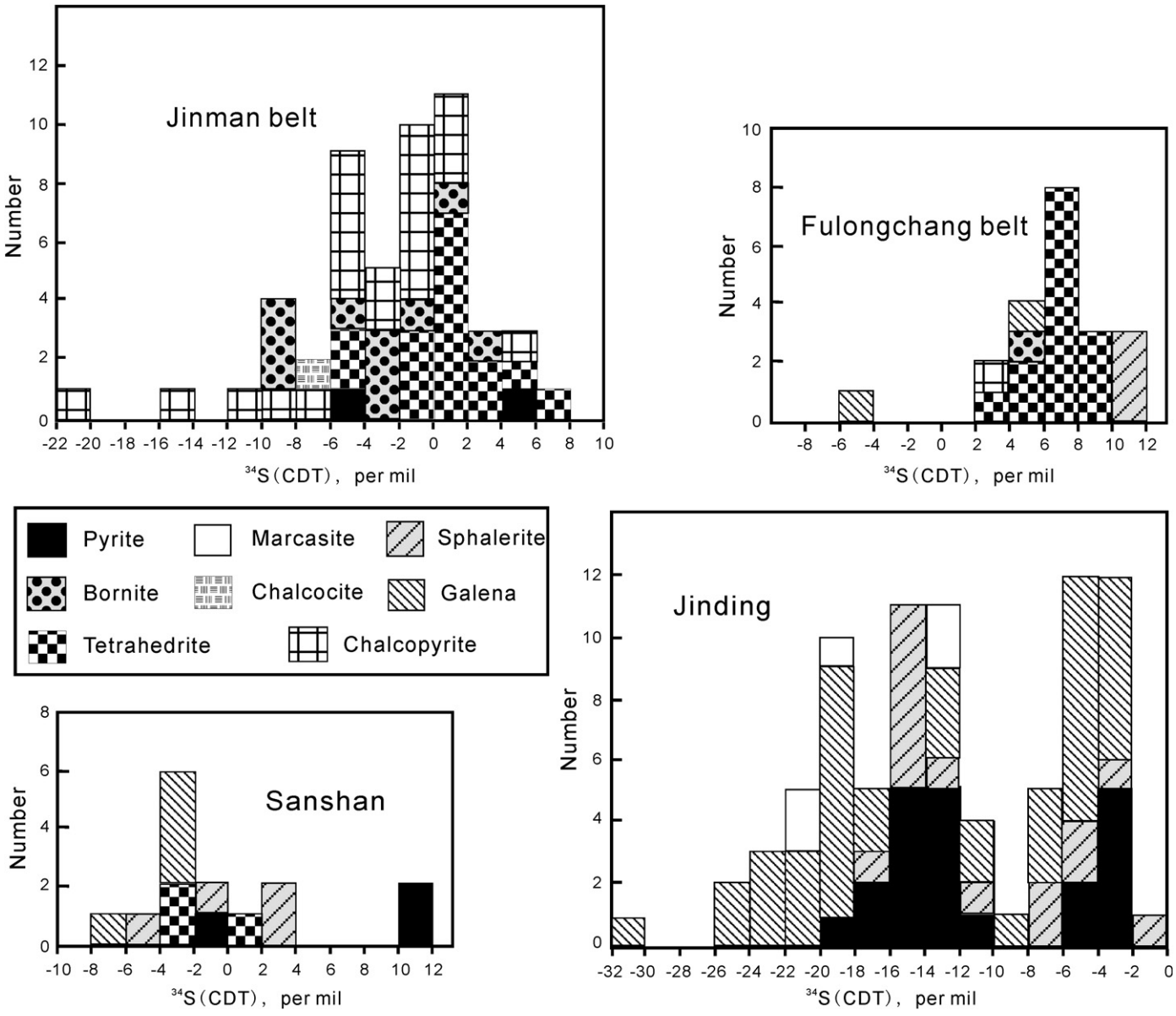

Fig. 15. Histogram of sulfur isotopic compositions of ore sulfides from the ore belts/deposits in the Lanping basin, also showing lead isotopic compositions of various rocks in the basin. Data are listed in Table 4.

15.9‰ (mean 12.5‰) for the Jinman ore belt, −2.5 to 18.2‰ (mean 5.9‰) for the Fulongchang ore belt, 6.5 to 24.3‰ (mean 15.9‰) for the Sanshan deposit, and 22.4 to 23.7‰ (mean 23.3‰) for the Jinding deposit.

In the $\delta^{13}C$–$\delta^{18}O$ plot (Fig. 17), there are two distinct arrays for the most deposits. The horizontal array include most deposits from the Jinman, Sanshan and Fulongchang belts, mostly plotted in a in the field between magmatic (carbonatic, mafic and felsic) carbon and marine carbonates (Fig. 17). They are characterized by a relatively narrow variation in $\delta^{13}C$ values, but much wide variation in $\delta^{18}O$. The vertical array is represented by the Jinding deposit, which yielded the lightest $\delta^{13}C$ and the heaviest $\delta^{18}O$ values, close

Notes to Table 4:
Min. — Host mineral. Cpy — Chalcopyrite; Sphal. — Sphalerite; Mar. — Marcasite; Tetrah. — Tetrahedrite. Superscripts of a to g represent the names of ore deposits (see Table 2). The data of Xiao (1989), Li et al. (1997), Liu et al. (2001), Wei (2001), Wang and He (2003) were obtained using a MAT251 mass spectrometer at Yichang Institute of Geology and Mineral Resources, with the precision better than 0.1‰. The data of Ji and Li (1998), He et al. (2004a), Zhao (2006), Li et al. (2005), and Ye et al. (1992) were obtained using a MAT253 mass spectrometer at Laboratory of Stable Isotope Geochemistry, Institute of Mineral Resources, CAGS, with the precision better than 0.2‰. The data of Wu et al. (2003) were determined by using a MAT251 mass spectrometer in the State Key Laboratory of Mineral Deposits Research, Nanjing University, with the precision better than 0.2‰. The data of Li et al. (2005) were obtained using a MAT252 mass spectrometer at Centre of Mineral Resources and Environment Research, Institute of Geochemistry, CAS, with the precision better than 0.2‰. The data of Zhang (1993) were derived using a MAT261 mass spectrometer at Beijing Research Institute of Uranium Geology, with the precision better than 0.2‰. In those laboratories, the $\delta^{34}S$ value of sulfide were measured on SO_2 released by placing the sulfide-CuO composite into a vacuum system heated to >1000 °C. Zhou and Zhou (1992) do not describe how their data was obtained — precision is difficult to evaluate.

Please cite this article as: He, L., et al., Thrust-controlled, sediment-hosted, Himalayan Zn–Pb–Cu–Ag deposits in the Lanping foreland fold belt, eastern margin of Tibetan Plateau, Ore Geology Reviews (2008), doi:10.1016/j.oregeorev.2008.11.001

Table 5
Hydrogen and oxygen isotopic compositions of fluid inclusions from hydrothermal quartz and calcite in ore deposits of the Lanping basin

Sample	Min.	δD_{H2O}, SMOW, ‰	$\delta^{18}O_{H2O}$, SMOW, ‰	Sample	Min.	δD_{H2O}, SMOW, ‰	$\delta^{18}O_{H2O}$, SMOW, ‰	Sample	Min.	δD_{H2O}, SMOW, ‰	$\delta^{18}O_{H2O}$, SMOW, ‰
Jinman ore belt											
After Li et al. (1995)				After Ji and Li (1998)				After Li et al. (2004)			
ZK1505-4[a]	Calc.	n.d.	4.23	Y-11 [a]	Qz	−109.4	−4.84	y-12 [a]	Qz	−30.3	4.2
	Calc.	n.d.	4.15	JM-1 [a]	Qz	−51	5.4	jm-1 [a]	Qz	−107	4.1
YM-1 [a]	Qz	−94.7	4.02	JM-18 [a]	Qz	−101	7.3	by-7 [a]	Calc.	−86.2	−10.3
TC-5 [a]	Qz	−73.8	3.63	JM-29 [a]	Qz	−86	5.2	w-1 [a]	Calc.	−62.6	−8.9
JL30-2 [a]	Qz	−63.4	9.77	JM-34 [a]	Qz	−102	4.4	After Zhao (2006)			
D-2 [p]	Calc.	−95.9	−1.89	LC-3 [a]	Qz	−95	7.0	JMIII-17 [a]	Qz	−112	9.3
D-12 [p]	Calc.	−102.9	−0.75	LK-5 [a]	Qz	−99.1	3.64	Nq-4 [r]	Qz	−57	3.7
SC-4 [j]	Qz	−83.8	4.5	K1505-2 [a]	Qz	−95.4	4.34	FC3-2 [s]	Qz	−120	5.7
SC-25 [j]	Qz	−78.8	1.34	After Liu et al. (2000)				DSQ1-1 [t]	Qz	−113	9.8
After Ji and Li (1998)				J3-2 [a]	Qz	−63	8.4	LZP1-1 [k]	Calc.	−118	2.1
JL30-1 [a]	Qz	−70.7	0.11	J3-1 [a]	Qz	−71	n.d.	RDH2-2 [l]	Calc.	−107	7.9
JZ3-16 [a]	Qz	−82.3	−5.14	J3-16 [a]	Qz	−82	3.4				
L5-3 [a]	Qz	−135.6	−10.57	L2-5 [q]	Qz	−87	5.5				
L2-5 [a]	Qz	−86.7	−1.76	v-11 [q]	Qz	−109	6.6				
Fulongchang ore belt											
After Gong et al., 2000				After Li et al., 2005				After Zhao, 2006			
B-6 [e]	Calc.	−109	−14.79	HX-24 [e]	Calc.	−76	−7.6	By-7 [e]	Calc.	−86	−10.3
B-10 [e]	Calc.	−103	−13.53	HX-25-1[e]	Calc.	−94	−7.5		Calc.	−87	−10.4
B-1 [e]	Qz	−97	−10.54	HX-26 [e]	Calc.	−94	−7.3	LL3-2 [u]	Calc.	−103	10.0
After Li et al., 2005				HX-27 [e]	Calc.	−93	−8.4				
ELC-142 [e]	Calc.	−94	−7.8	HX-30 [e]	Calc.	−100	−8.3				
Sanshan ore deposit											
After Chen et al., 2004				After Chen et al., 2004				After Zhao, 2006			
H95	Qz	−88.6	−0.65	H142	Calc.	−78.7	−10.92	HCS1-2	Calc.	−122	−1.3

Notes: Min. — Host mineral. Calc. — Calcite; Qz — Quartz. Superscripts of a to u represent the names of ore deposits: a to o are as same as in Tables 2 and 3. p — Dahua; q — Liancheng; r — Enqi; s — Fengchuan; t — Dashanqing; u — Lailong. The data of Li et al. (1995), Liu et al. (2000), and Chen et al. (2004) were obtained using a MAT251 mass spectrometer at Yichang Institute of Geology and Mineral Resources, with precision better than 0.2‰ for $\delta^{18}O$ and 2‰ for δD. The data of Li et al. (2004), Gong et al. (2000), and Li et al. (2005) were determined by a MAT253 mass spectrometer at Laboratory of Stable Isotope Geochemistry, Institute of Mineral Resources, CAGS, with precision better than 0.2‰ for $\delta^{18}O$ and 2‰ for δD. $\delta^{18}O$ values with precision better than 0.2‰ of Ji et al. (1998) were obtained using a MAT253 mass spectrometer at Laboratory of Stable Isotope Geochemistry, Institute of Mineral Resources, CAGS, whereas δD values with the precision better than 2‰ of Ji and Li (1998) were determined by a MAT251 mass spectrometer at Yichang Institute of Geology and Mineral Resources. The data of Zhao (2006) were determined by MAT261 at Laboratory for Stable Isotope Geochemistry, Institute of Geology and Geophysics, CAS, with precision better than 0.2‰. The $\delta^{18}O$ values of quartz were initially determined on CO_2 through graphite reacting with O_2 generated from the reaction between quartz and BrF_5. Then, the $\delta^{18}O_{H2O}$ values were calculated from those of quartz on the basis of the isotope fractionation equation of 1000 $\ln\alpha_{quartz\text{-}water}=3.42\times10^6\,T^{-2}-2.86$ (Zhang, 1985) at the homogenisation temperatures of associated fluid inclusions. The $\delta^{18}O$ values of calcite were determined on CO_2 extracted from carbonates by reaction with phosphoric acid. The $\delta^{18}O_{H2O}$ values were then calculated from those of calcite on the basis of the isotope fractionation equation of 1000 $\ln\alpha_{calcite\text{-}water}=2.78\times10^6\,T^{-2}-3.39$ (O'Neil et al., 1969) at the homogenization temperatures of associated fluid inclusions. The δD_{H2O} values were obtained from water released by thermal decrepitation of fluid inclusions.

to the field of sedimentary organisms (Fig. 17). These data suggest that ore-forming fluids for these deposits have distinct sources of carbon.

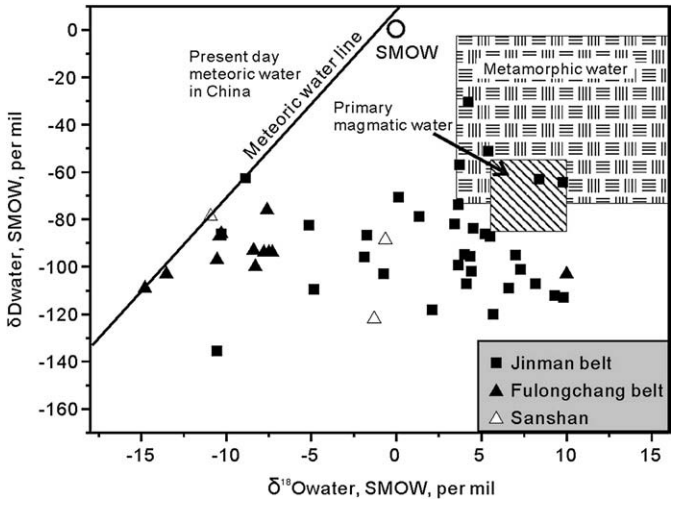

Fig. 16. Plot of δD *vs.* $\delta^{18}O$ of water in fluid inclusions from hydrothermal quartz and calcite in the ore belts/deposits of the Lanping basin. The equation of the meteoric water line is "$\delta D=7.9\,\delta^{18}O+8.2$" (Chen and Wang, 2004). The field of primary magmatic water is calculated for water in equilibrium with "normal" igneous rocks at ≥700 °C (Misra, 2000). The field of metamorphic water is calculated for water in equilibrium with silicate minerals at T=300 to 600 °C (Misra, 2000). Data are listed in Table 5.

8. Discussion and conclusions

8.1. Age of mineralization

The age of mineralization in the Lanping foreland fold belt has been much debated, although considerable efforts have recently been made using various dating methods. For example, an age of 67 Ma was obtained from Re–Os dating of ore pyrite from the Jinding deposit (Xue et al., 2003) and two $^{40}Ar/^{39}Ar$ ages (63–60 Ma and 56.53±0.43 Ma) were obtained by step heating ^{39}Ar–^{40}Ar dating on fluid inclusions in hydrothermal quartz from the Baiyangping deposit (Xue et al., 2003; He et al., 2004b). However, these ages are apparently unreasonable (Xue et al., 2007) because the mineralization occurs within Paleocene strata (E_1y). Similarly, in the Jinman deposit, ^{39}Ar–^{40}Ar dating on hydrothermal quartz gave ages of 58 to 54 Ma (Liu et al., 2003) and 56.7±1.0 Ma (Xu et al., 2004), and ^{39}Ar–^{40}Ar analysis of hydrothermal sericite yielded ages of 87, 67 and 37 Ma, whereas K–Ar dating on hydrothermal illite yielded ages of 46.71±0.68 Ma (Bi and Mo, 2004), and 47 to 40 Ma and 36 to 35 Ma (Zhao, 2006). Due to the excess Ar that is usually contained in fluid inclusions, the ages obtained by ^{39}Ar–^{40}Ar dating on guange quartz are probably older than real age of mineralization. Similarly, considering that clastic illites and sericites from country rocks are easily interfused into illites and sericites of hydrothermal alteration origin, the ages obtained by the K–Ar or ^{39}Ar–^{40}Ar techniques are probably contaminated, giving ages that are too old. However, as discussed below, it is most likely that the youngest of the three ages might represent the age of main mineralization (Wang et al., 2005).

Please cite this article as: He, L., et al., Thrust-controlled, sediment-hosted, Himalayan Zn–Pb–Cu–Ag deposits in the Lanping foreland fold belt, eastern margin of Tibetan Plateau, Ore Geology Reviews (2008), doi:10.1016/j.oregeorev.2008.11.001

Table 6
Carbon and oxygen isotopic compositions of hydrothermal carbonate minerals from ore deposits in the Lanping basin

Sample	Min.	$\delta^{13}C$, PDB ‰	$\delta^{18}O$, SMOW ‰	Sample	Min.	$\delta^{13}C$, PDB ‰	$\delta^{18}O$, SMOW ‰	Sample	Min.	$\delta^{13}C$, PDB‰	$\delta^{18}O$, SMOW ‰
Jinman ore belt											
After Yan (1993)				After Li et al. (1995)				After Liu et al. (2001)			
Jd-1-2 [a]	Calc.	−4.89	14.19	JD-1-1 [a]	Dol.	−4.92	15.33	y-12 [a]	Calc.	−7.4	15.9
	Dol.	−4.92	14.61	JD-1-2 [a]	Calc.	−4.89	15.33	After Xu and Li (2003)			
After Li et al. (1995)				D-2 [p]	Calc.	−5.25	5.34	s01134 [a]	Calc.	−6.6	15.54
ZK1505-4 [a]	Calc.	−4.83	14.41	D-12 [p]	Calc.	−5.07	7.93				
	Calc.	−4.83	14.34		Dol.	−5.26	4.19				
Fulongchang ore belt											
After Chen et al. (2000)				After Xue et al. (2002)				After Xu and Li (2003)			
H-84 [e]	Calc.	−4.16	18.2	BYP-91[e]	Calc.	−1.2	4.5	ss01190 [h]	Calc.	−1.90	10.24
H-85 [e]	Sid.	−2.95	15.1	BYP-93 [e]	Calc.	−1.9	−0.5	After Liu et al. (2004)			
H-72 [d]	Calc.	−2.31	13.5	After Xue et al. (2002)				HX-24 [e]	Calc.	−1.9	0.9
H-74 [d]	Sid.	−3.1	16.3	BYP-143 [e]	Calc.	−2.4	−0.2	HX-25-1 [e]	Calc.	−2.3	1.1
H-76 [d]	Sid.	−3.2	16.4	BYP-152 [e]	Calc.	−2.3	−0.3	HX-26 [e]	Calc.	−1.1	1.3
H-78 [d]	Calc.	−3.11	16.3	BYP-161 [e]	Calc.	−3.0	−0.6	HX-27 [e]	Calc.	−1.9	0.2
H-79-1 [d]	Calc.	−2.78	17.4	BYP-181 [e]	Calc.	−3.0	−2.5	HX-30 [e]	Calc.	−0.5	0.2
H-79-2 [d]	Calc.	−3.08	15.8	BYP-8 [e]	Calc.	−0.8	0.6	By-7-1 [e]	Calc.	−1.7	0.0
After Gong et al. (2000)				BYP-9 [e]	Calc.	−1.5	−0.2	By-7-2 [e]	Calc.	−1.7	−0.1
B-6 [e]	Calc.	n.d.	15.66	BYP-15 [e]	Calc.	−2.2	0.8	w-1[h]	Calc.	−1.9	1.5
B-10 [e]	Calc.	n.d.	16.96	BYP-16 [e]	Calc.	−1.4	0.5	Lzp109 [k]	Calc.	−2.4	1.4
After Xue et al. (2002)				BYP-17 [e]	Calc.	−1.2	−0.3	Lzp109 [k]	Calc.	−3.3	14.1
BYP-5 [e]	Calc.	−1.9	−0.3	BYP-36 [e]	Calc.	−2.3	−0.4	Wdc105 [k]	Calc.	−2.9	12.0
BYP-6 [e]	Calc.	−2.4	−0.9	BYP-38 [e]	Calc.	−2.3	5.5	FLC142[d]	Calc.	−2.3	0.7
BYP-33 [e]	Calc.	−2.4	−0.2	After Xu and Li (2003)				After Zhao (2006)			
BYP-34 [e]	Calc.	−2.3	−0.3	ss97070 [e]	Calc.	−3.80	15.52	LL3-2 [u]	Calc.	2.3	15.5
BYP-81 [e]	Calc.	−1.9	−0.3	ss97072 [d]	Calc.	−3.87	16.82				
Sanshan ore deposit											
After Xue et al. (2002)				After Liu et al. (2004)				After Chen et al. (2000)			
H-12	Calc.	2.1	20.8	HX-32-1	Calc.	−7.6	15.9	H-17	Stron.	−5.45	14.3
H-14	Calc.	2.7	22.6	HX-32-2	Calc.	−7.6	16.0	H-23	Calc.	0.17	13.1
After Xu and Li (2003)				HX-48	Calc.	−3.6	20.3	H-53	Sid.+Calc.	−4.1	8.8
s01167	Calc.	−4.6	11.96	HX-51	Calc.	−2.4	21.3	H-54	Sid.+Calc.	0.67	16.5
s01172	Calc.	−4.86	9.63	hs116	Calc.	0.4	24.3	After Zhao (2006)			
ss97039	Calc.	2.11	6.46	hs101	Calc.	−2.3	16.9	HCS1-2	Calc.	2.5	10.8
After Liu et al. (2004)				Hxs102	Calc.	−8.3	19.8				
HX-31	Calc.	1.6	9.0	hxs105	Calc.	−3.7	22.7				
Jinding ore deposit											
After Luo et al. (1994)				After Luo et al. (1994)				After Luo et al. (1994)			
PBT1	Calc.	−20.9	23.6	TY209	Calc.	−11.9	22.4	TY207	Calc.	−24.4	23.2
JPTW3	Calc.	−6.1	23.6	TY208	Calc.	−24.5	23.7	TY208	Calc.	−24.5	23.4
JPTW4	Calc.	−18.0	23.3								

Notes: Min. — Host mineral. Calc. — Calcite; Stron. — Strontianite; Sid. — Siderite. The superscripts of a to u represent the names of ore deposits: the names of a to i are as same as those in Table 2, j to o are as same as those in Table 3, and P to u are as same those in Table 5.
The data of Yan (1993), Li et al. (1995), Liu et al. (2001), Chen et al. (2000) and Luo et al. (1994) were obtained using a MAT251 mass spectrometer at Yichang Institute of Geology and Mineral Resources, with the precision better than 0.2‰ for the $\delta^{13}C$ and $\delta^{18}O$. The data of Xu and Li (2003) were obtained using a MAT251 mass spectrometer at Analytic Centre, Chinese University of Geosciences (Wuhan) with the precision better than 0.2‰ for the $\delta^{13}C$ and $\delta^{18}O$. The data of Gong et al. (2000), Xue et al. (2002) were determined by a MAT253 mass spectrometer at Laboratory of Stable Isotope Geochemistry, Institute of Mineral Resources, CAGS, with the precision better than 0.2‰ for the $\delta^{13}C$ and $\delta^{18}O$. The samples HX-24, HX-25-1, HX-26, HX-27, HX-30, HX-31, HX-32-1, HX-32-2, HX-48, and HX-51 were analyzed using a MAT251 mass spectrometer at Centre of Mineral Resources and Environment Research, Institute of Geochemistry, CAS, with the precision better than 0.2‰ for the $\delta^{13}C$ and $\delta^{18}O$. The samples By-7-1, By-7-2, and w-1 were analyzed using a MAT251 mass spectrometer at Yichang Institute of Geology and Mineral Resources, with the precision better than 0.2‰ for the $\delta^{13}C$ and $\delta^{18}O$. The samples Lzp109, Lzp138, wdc105, hs116, hs101, hxs102, hxs105, and flc142 were analyzed using a MAT253 mass spectrometer at Laboratory of Stable Isotope Geochemistry, Institute of Mineral Resources, CAGS, with the precision better than 0.2‰ for the $\delta^{13}C$ and $\delta^{18}O$. The data of Zhao (2006) were determined by MAT261 at Laboratory for Stable Isotope Geochemistry, Institute of Geology and Geophysics, CAS, with the precision better than 0.2‰for the $\delta^{13}C$ and $\delta^{18}O$.
In those laboratories, the $\delta^{13}C$ and $\delta^{18}O$ values were determined on CO_2 extracted from carbonates by reaction with phosphoric acid.

The significant observation that the spatial localization of sulfide orebodies in the fold belt is controlled by the Cenozoic thrust–nappe systems indicates that these base metallic deposits were certainly formed after those strata involved in the systems. The E_1y stratum is regionally involved in the western or the eastern thrust–nappe systems (Figs. 4 and 5), suggesting a post-E_1y mineralization (i.e., ~56 Ma at the end of the Paleocene). The youngest mineralized stratum in the fold belt is the E_2b sequence, in which numerous mineral occurrences in the region are found, is unconformably overlain by younger strata. This suggests that the mineralization probably happened at the time of, or older than the interval represented by the unconformity i.e., ~34 Ma of the beginning of Oligocene (Fig. 3). In the region, a pseudo-conformity occurs between the E_1y unit and overlying Guolang Formation (E_2g), and unconformities are present between the E_2g and E_2b strata and between the E_2b and its overlying strata, respectively (Fig. 3; Mu et al., 1999). Mineralization could not have taken place during the period represented by the pseudo-conformity or sedimentation of the E_2g strata, because, if this was the case, the E_1y stratum should have been strongly deformed and there should be an unconformity between the E_1y and E_2g strata, which is not observed. It is thus reasonable to interpret formation of the deposits after deposition of the E_2g stratum. Regional geological investigation (Zhao, 2006) has established that the end of the E_2g is at ~40 Ma (beginning of the Late Eocene). We therefore argue that the mineralization ages are between ~40 Ma and ~34 Ma. The ages denote that these ore deposits are Himalayan, formed in the environment of a foreland basin within continent–continent collision orogen (Wang et al., 2001; Spurlin et al., 2005; Li et al., 2006a; Hou et al., 2006).

Please cite this article as: He, L., et al., Thrust-controlled, sediment-hosted, Himalayan Zn–Pb–Cu–Ag deposits in the Lanping foreland fold belt, eastern margin of Tibetan Plateau, Ore Geology Reviews (2008), doi:10.1016/j.oregeorev.2008.11.001

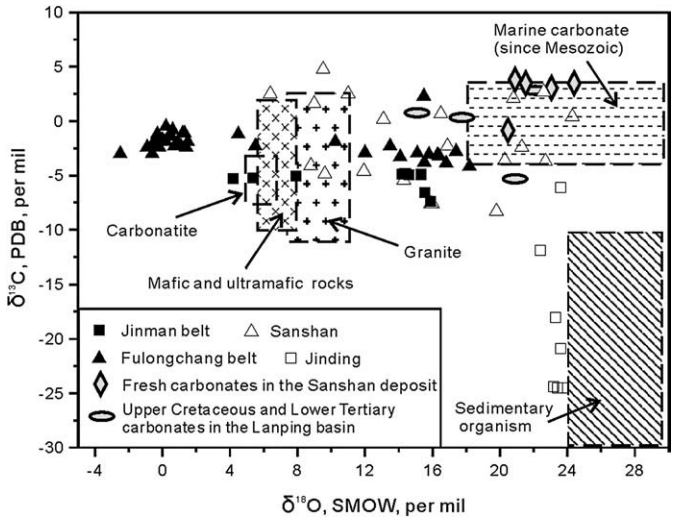

Fig. 17. Plot of $\delta^{13}C$ *vs.* $\delta^{18}O$ of hydrothermal carbonate minerals from the ore belts/deposits in the Lanping basin, also showing $\delta^{13}C$ and $\delta^{18}O$ values of the carbonates in the basin. The fields of carbonatite, mafic and ultramafic rocks, granite, marine carbonate, and marine and non-marine sedimentary organisms are approximately plotted based on the data in Misra (2000), and Chen and Wang (2004). Data are listed in Table 6.

8.2. Role of the thrust systems in mineralization

Three genetic links between the thrust systems and mineralization can be recognized in the Lanping fold belt. Firstly, the thrust systems generate open spaces for ore accumulation. At a deposit scale, many vein or lens orebodies are hosted in thrust faults. Ore textures are predominantly those resulting from open-space filling, such as cavity-filling, fracture-filling, filling of inter-fragment open spaces in breccias, as well as cementation textures. At the regional scale, the deposits are assigned mainly to the front zones of the thrust systems. The Jinding and Sanshan deposits occur in the front zones of the eastern thrust–nappe system, whereas the Fulongchang ore belt lies in the equivalent zone of the western thrust–nappe system. A possible interpretation is that the front zone usually generates numerous second-order faults and structural fractures, consequently providing a large amount of open spaces for convergence of fluid flows and precipitation of sulfides.

Secondly, the thrust systems provide potential migration paths for ore-forming fluids derived from brine basins (see below). Long-distance lateral migration of ore-forming fluids can be realized through stable permeable aquifers at deep-structural levels in the case of MVT Pb–Zn deposits because they are commonly formed in mildly deformational basins (Sverjensky, 1986; Garven, 1985, 1989, 1995). Such paths are, unfortunately, hardly inapplicable for the Lanping basin on account of the strong syn-mineralization deformation. The deformation, in terms of thrust–nappe structures, leads however to the formation of faults and folds, which are most unlikely to have permittd long-distance lateral migration of fluid flows through strongly-folded permeable aquifers. In a thrust system, however, a gently-dipping detachment fault zone, which possibly existed at deep-structural levels, might be considered as highly permeable and may have acted as good lateral fluid migration path. On the other hand, the thrust faults, downward connecting to the detachment fault zone, could themselves have provides channel ways for upward discharge of ore-forming fluids.

Thirdly, the thrust systems may themselves represent trap structures for the accumulation of minerals deposited from the ore-

Table 7
Comparison of main characteristics of the Zn–Pb–Cu–Ag deposits in the Lanping basin (Lanping-type), MVT-, SST-, SSC-, and SEDEX-type deposits

	Lanping-type	MVT	SST	SSC	SEDEX
Tectonic setting	Foreland basin in continent–continent collision orogen	Foreland basin, continental rift basin	Stable tectonic settings in continental interior or margin	Continental rift basin	Intracontinental or failed rifts and rifted continental margins
Basin during mineralization	Strongly deformed	Undeformed, mildly deformed, rarely strongly deformed	/	Undeformed redbed-bearing basin	/
Host rocks	Sedimentary rocks, but no selection for the rock types	Carbonates	Quartz-rich sandstone	Mainly carbonaceous shales, marls, arenites	Dolostones, limestone or marble within overall siliciclastic sequences, shales and cherts, dolomitic siltstones, pyritic siltstones and greywackes
Ore controls	Thrust-related faults, thrust-related lithologic trap	Lithology, carbonate dissolution collapse structure, fault/fracture	Basal unconformity and permeability of rocks	Oxidized and reduced nature of strata	Broad paleotopographic highs and domal structures, syndepositional faults with talus breccias, localized facies variations and/or thickening in sub-basins
Orebody morphology	Vein, concordant with fault	Highly variable, usually strata-bound	Lensoid, conformable to bedding in sandstone	Stratiform	Tabular, stratiform and stacked lensoid, minor in stock work and vein in footwall
Ore texture	Vein, minor in disseminated	Vein, massive, commonly coarse grained sulfides	Disseminated	Fine-grained disseminated	Commonly laminated fine grained sulfides
Typical minerals	Sphalerite, galena, tetrahedrite, calcite, dolomite, barite, celestite	Sphalerite, galena, dolomite, and calcite	Galena, minor sphalerite and chalcopyrite	Chalcocite, bornite, chalcopyrite, and pyrite	Sphalerite, galena, pyrite, pyrrhotite, barite, and chert
Mineralization style	Open-space filling, breccias-cementing, minor in replacement	Open-space filling, breccias- cementing, minor in replacement	Cementation, open-space filling	Syndiagenetic mineralization, cementation	Syndiagenetic or synsedimentary mineralization
Economic metals	Zn, Pb, Cu, Ag, Zn>Pb	Pb, Zn	Pb, Zn, Pb>Zn, minor amounts of Cu	Cu-dominated, Pb, Zn, Ag, and Co in some deposits	Pb, Zn, a certain amount of Cu
Ore-forming fluids	Temperatures of <200 °C and salinities of 1–28 wt. % NaCl eq.	Temperatures of typical 90–200 °C and salinities of 10–30 wt.% NaCl eq.	/	Temperatures of <100 °C	Temperatures of typical 90–200 °C and salinities of 10–30 wt.% NaCl eq.
Magmatic affiliation	Lack	Lack	Lack	Lack	Lack

Note: The features of MVT-, SST-, SSC-, and SEDEX-type ore deposits mainly refer to the book compiled by Misra (2000) and the paper of Leach et al. (2005).
'/' denotes that the authors know less about the associated content.

Please cite this article as: He, L., et al., Thrust-controlled, sediment-hosted, Himalayan Zn–Pb–Cu–Ag deposits in the Lanping foreland fold belt, eastern margin of Tibetan Plateau, Ore Geology Reviews (2008), doi:10.1016/j.oregeorev.2008.11.001

forming fluids. A typical example is the Jinding deposit, in which the F_2 thrust fault and its hanging- and footwall rocks operated as a trap. In fact, the mud- and siltstone sequences of the Huakaizuo Formation overlying the orebody are also important to the formation of sulfide ores, these sequences have low permeability and, consequently, may have acted as a hydraulic barrier prevented further upwards flow of the ore-forming fluids.

8.3. Sources of ore-forming fluids and materials

Fluid inclusions from ore deposits in the Lanping basin have homogenization temperatures (T_h) that vary from 54 to 309 °C, but which are commonly <240 °C (Fig. 11). Salinities range from 1.0 to 28.0 wt.% NaCl equiv. (Fig. 12). Conservatively, the data for sphalerite gives temperatures from 110 to 240 °C and salinities of 4 to 21 wt.% NaCl equiv. (Figs. 11 and 12). The low-T and high-salinity characters imply that the ore-forming fluids in the Lanping basin are distinguished from magmatic water with >300 °C, as well as from meteoric or seawater with low salinities (normally <5 wt.% NaCl equiv.). The H–O isotopes of fluid inclusions predominately lie in the field between the meteoric water line (MWL) and magmatic (and metamorphic) water (Fig. 16), thus eliminating meteoric water, magmatic, or metamorphic waters as the sole source of ore-forming fluids. This is consistent with fact that no recognizable igneous or metamorphic activity occurred in the north of the Lanping basin during the Himalayan stage.

There are several lines of evidence to suggest basinal brines as the source of ore-forming fluids in the Lanping basin. Firstly, the fluid inclusions of these deposits have salinities from 10 to 30 wt.% NaCl equiv. and temperatures mainly within the range 90 to 200 °C, at least similar to fluids from MVT and SEDEX deposits (Leach et al., 2005). Secondly, they have $^{18}O/^{16}O$ ratios that range from meteoric to higher than meteoric (Misra, 2000), which are basically consistent with those of the fluids in the Lanping basin. Third, C–O isotope systematics in the Lanping deposits are generally characterized by higher $\delta^{18}O$ and lower $\delta^{13}C$, which require involvement of marine carbonates and sedimentary organisms in the basin to supply carbon and oxygen (Fig. 17). The likelihood that at least some of the carbon and oxygen are basin-derived is also consistent with the C–O isotopic data of some hydrothermal carbonate minerals in Lanping, which are similar to those of "marine carbonates" (Fig. 17). In addition, the fact that hydrocarbon-rich fluid inclusions are found in gangue minerals (Fig. 10) also testifies to the probability that basinal brines were the source (s) of ore-forming fluids. The widely distributed evaporite sulfates in the Lanping basin may have provided salts for the brines. Comparing with typical basinal brines, some fluid inclusions in the Lanping basin yielded relatively lower salinities (<10 wt.% NaCl equiv.). However, these low-salinity inclusions show a positive correlation with their T_h values, suggesting a possible mixing between meteoric water and basinal brines.

The ore deposits in the basin display wide variations in sulfide $\delta^{34}S$ values (Fig. 15), indicating multiple sulfur sources. On account of the lack of magmatic activity, it is realistic to view the rocks in the Lanping basin as the source of sulfur. These include evaporite (positive $\delta^{34}S$ values), the strata enriched in organic sulfur (slightly positive to negative $\delta^{34}S$ values), and sedimentary rocks containing diagenetic pyrite (very positive to very negative $\delta^{34}S$ values) (Misra, 2000). Sulfur in the rocks was transferred into hydrothermal fluids via fluid-rock interaction. Therefore, the variation in rock types across the basin is likely to influence the variation of sulfur isotopic compositions in the different deposits.

Lead isotopic compositions also suggest that ore-forming metals originated from rocks of the Lanping basin, because almost all Pb isotopic data plot within the field of crustal Pb isotopes of the basin (Fig. 14a, b) — this is especially true for the Jinman, Fulongchang, and Sanshan ore belts/deposits. Their Pb isotopic compositions are similar to those main sedimentary rocks in the basin. The Jinding deposit has totally different Pb isotopes from the other deposits. Although Xue et al. (2007) argued that the lead is predominately derived from the mantle, other possibilities cannot be ruled out. On Fig. 14a, b, most of the Pb isotopes of the Jinding deposits are still located in the field of crustal Pb isotopes of the Lanping basin, similar to those of mafic, ultramafic, and alkaline rocks. Geochemical study (e.g., La/Th, U/Th, δCe, and δEu) on the cement of the Paleocene detrital rocks around the Jinding area suggested that the source materials of these rocks result from mixing of felsic, mafic–ultramafic rocks with deep brines (Li et al., 2006b). Accordingly, we interpret that the lead of the Jinding deposit was mainly derived from the sedimentary rocks rich in mafic and ultramafic detrital materials in the Jinding area.

8.4. Comparison with MVT, SST, SSC and SEDEX type deposits

Table 7 summarizes the main characteristics of the deposits in the Lanping basin (which we term 'Lanping-type'), MVT-, SST-, SSC-, and SEDEX-type deposits. All are broadly viewed as having formed from fluids derived from sedimentary basins and show no affinity to magmatic activity. Lanping-type deposits are similar to MVT deposits in that the ore-forming fluids are mainly derived from basinal fluids, and are characterized by formation temperatures of (mainly) <200 °C and salinities up to more than 10 to 20 wt.% NaCl equiv. In addition, both share similar mineralization styles with a dominance of open-space filling and breccia cementation, indicative of epigenetic mineralization. Moreover, they are similar in that mineral constituents are dominated by sphalerite, galena, calcite, and dolomite. However, Lanping-type deposits are typically thrust fault-controlled and show no preference for host rock type, whereas MVT-type deposits are controlled by lithology and faulting/fracturing with a strong preference for carbonates host rocks (Leach et al., 2005). Furthermore, the bulk composition of Lanping-type deposits, which besides Zn, Pb and Ag, are also rich in Cu, differs from that of MVT deposits. With respect to tectonic setting, Lanping-type deposits occur in a strongly deformed foreland basin within a continental collision zone, whereas the vast majority of MVT deposits were formed in mildly-deformed or undeformed sedimentary basins from foreland or continental rift. It should be pointed out, however, that a few MVT deposits were also generated in strongly deformed basins, e.g., in the Picos de Europa district, Northern Spain and the Canadian Rockies thrust belt (Bradley and Leach, 2003). Similar to the Lanping area, mineralization was coeval with, or postdated thrust systems, so further comparison is valuable for understanding the hydrologic setting of Lanping-type deposits.

Lanping-type deposits share some similarities with SST-type deposit in terms of the lack of magmatic affinity, ore-forming fluids, and mineralization style. However, Lanping-type deposits are, firstly, controlled by thrust–nappe systems, whereas SST deposits are closely related to basal unconformities and strata permeability and are prone to occurring in quartz-rich sandstone within basin basement. Secondly, the active tectonic setting of Lanping-type deposits differs from the relatively stable tectonic setting of SST deposits. Thirdly, Lanping-type deposit contain a variety of sulfides, generally with Zn>Pb; SST deposits always have Pb>Zn.

Lanping-type deposits apparently differ from SSC deposits, because the latter represent syn-diagenetic mineralization and ore-forming fluids show temperatures <100 °C. In addition, SSC deposits tend to occur in basins rich in redbeds and evaporites, with the boundary between oxidized and reduced facies representing as the most favorable location for ore accumulation.

There are remarkable discrepancies between Lanping-type and SEDEX deposits, although they both have no clear affinity with magmatic rocks and contain Pb, Zn and Cu. Typically, Lanping-type deposits are epigenetic relative to host rocks, whereas SEDEX deposits are of syndiagenetic exhalative-sedimentary genesis and have ore

Please cite this article as: He, L., et al., Thrust-controlled, sediment-hosted, Himalayan Zn–Pb–Cu–Ag deposits in the Lanping foreland fold belt, eastern margin of Tibetan Plateau, Ore Geology Reviews (2008), doi:10.1016/j.oregeorev.2008.11.001

textures which are laminated conformable to the bedding of the host rocks.

In summary, although Lanping-type deposits share some similarities with MVT, SST, SSC, and SEDEX ore deposits, they cannot be fully satisfactorily classified within any of them. Lanping-type deposits have a number of distinguishing features, including: (1) formation in a strongly deformed foreland basin within a continent–continent collisional orogen; (2) they are closely related to thrust–nappe structures; (3) they are fault-controlled, without strong selection for type of host rocks; and (4) contains a variety of metals (Zn, Pb, Cu, Ag, Sr, Co etc.). Therefore, we suggest that the Himalayan Zn–Pb–Cu–Ag deposits controlled by the thrust systems in the Lanping basin represent a new deposit type.

Acknowledgements

The study was funded by the National Basic Research Plan 973 Project (2002CB41260 to Z.Q. Hou) and by the Outstanding Youth Foundation of NSF of China (40425014 to Z.Q. Hou), Special Foundation from (former) Ministry of Geology and Mineral Resources of China (No.98-13 to L.Q. He), China Postdoctoral Science Foundation (20070420418 to Y.C. Song), and Basic Outlay of Scientific Research Work from Ministry of Science and Technology of China (J0723 to Y.C. Song).

References

Bai, J.F., Wang, C.H., Na, R.X., 1985. Geological characteristics of the Jinding lead-zinc deposit in Yunnan with a special discussion on its genesis. Mineral Deposits 4, 1–9 (in Chinese with English abstract).

Bi, X.M., Mo, X.X., 2004. Transition from diagenesis to low-grade metamorphism and related minerals and energy resources. Earth Sciences Frontiers 11, 287–294 (in Chinese with English abstract).

Bjørlykke, A., Sangster, D.F., 1981. An overview of sandstone lead deposits and their relation to red-bed copper and carbonated hosted lead-zinc deposits. Economic Geology 76, 179–213.

Bradley, D.C., Leach, D.L., 2003. Tectonic controls of Mississippi Valley-type lead-zinc mineralization in orogenic forelands. Mineralium Deposita 38, 652–667.

Chen, K.X., He, L.Q., Yang, Z.Q., Wei, J.Q., Yang, A.P., 2000. Oxygen and carbon isotope geochemistry in Sanshan-Baiyangping copper-silver polymetallogenic enrichment district, Lanping, Yunnan. Geology and Mineral Resources of South China 4, 1–8 (in Chinese).

Chen, K.X., Yao, S.Z., He, L.Q., Wei, J.Q., Yang, A.P., Huang, H.L., 2004. Ore-forming fluid in Baiyangping silver-polymetallic mineralization concentration field in Lanping, Yunnan Province. Geological Science and Technology Information 23, 45–50 (in Chinese with English abstract).

Chen, K.X., 2006. The forming mechanism of copper-silver polymetallic ore concentration area in the north of Lanping forelandbasin in Yunnan Province. Ph.D Dissertation, China University of Geosciences, Beijing, 128 pp. (in Chinese with English abstract).

Chen, J., Wang, H.N., 2004. Geochemistry. Science Press, Beijing. 129 pp. (in Chinese).

Chung, S.L., Lo, C.H., Lee, T.Y., Zhang, Y.Q., Xie, Y.W., Li, X.H., Wang, K.L., Wang, P.L., 1998. Dischronous uplift of the Tibetan Plateau starting from 40 Ma ago. Nature 349, 769–773.

Dong, F.L., Mo, X.X., Hou, Z.Q., Wang, Y., Bi, X.M., Zhou, S., 2005. ^{40}Ar~^{39}Ar ages of Himalayan alkaline rocks in Lanping basin, Yunnan Province, and their geological implications. Acta Petrologica et Mineralogica 24, 103–109 (in Chinese with English abstract).

Gao, Z.Q., Zhao, Q.H., Tong, Y.H., 2006. Jinman sedimentation-hydrothermal reformation Cu deposit, Lanping. Journal of Yunnan Geology 25, 341–347 (in Chinese with English abstract).

Garven, G., 1985. The role of regional fluid flow in the genesis of the Pine Point deposit, Western Canadian Sedimentary basin. Economic Geology 80, 307–324.

Garven, G., 1989. A hydrogeological model for the formation of the giant oil sands deposits of the Western Canada Sedimentary Basin. American Journal of Science 289, 105–166.

Garven, G., 1995. Continental-scale groundwater flow and geological processes. Annual Review of Earth and Planetary Sciences 23, 89–117.

Gong, W.J., Tan, K.X., Li, X.M., Gong, G.L., 2000. Geochemical characteristics of fluid and mechanism for ore formation in the Baiyangping copper–silver deposit, Yunnan. Geotectonica et Metallogenia 24, 175–181 (in Chinese with English abstract).

He, L.Q., Chen, K.X., Yu, F.M., Wei, J.Q., Yang, A.P., Li, H., 2004a. Nappe tectonics and their ore-controlling of Lanping basin in Yunnan Province. Geology and Prospecting 40, 7–12 (in Chinese with English abstract).

He, M.Q., Liu, J.J., Li, C.Y., Li, Z.M., Liu, Y.P., 2004b. Mechanism of ore-forming fluids of the Lanping Pb–Zn–Cu polymetallic mineralized concentration area— an example study on the Baiyangping ore district. Geological Publishing House, Beijing. 117 pp. (in Chinese).

He, M.Q., Liu, J.J., Li, C.Y., Li, Z.M., Liu, Y.P., Yang, A.P., Sang, H.Q., 2006. ^{40}Ar~^{39}Ar dating of ore quartz from the Baiyangping Cu–Co polymetallic mineralized concentration area, Lanping, Yunnan. Chinese Journal of Geology 41, 688–693 (in Chinese with English abstract).

Hou, Z.Q., Hou, L.W., Ye, Q.T., Liu, F.L., Tang, G.G., 1995. Tectono-magmatic evolution and volcanogenic massive sulphide deposits in the Yidun island-arc, Sanjiang Region, China. Earthquake Publishing House, Beijing. 218 pp. (in Chinese).

Hou, Z.Q., Ma, H.W., Khin, Z., Zhang, Y.Q., Wang, M.J., Wang, Z., Pan, G.T., Tang, R.L., 2003. The Himalayan Yulong porphyry copper belt: product of large-scale strike-slip faulting in eastern Tibet. Economic Geology 98, 125–145.

Hou, Z.Q., Pan, G.T., Wang, A.J., Mo, X.X., Tian, S.H., Sun, X.M., Ding, L., Wang, E.Q., Gao, Y. F., Xie, Y.L., Zeng, P.S., Qin, K.Z., Xu, J.F., Qu, X.M., Yang, Z.M., Yang, Z.S., Fei, H.C., Meng, X.J., Li, Z.Q., 2006. Metallogenesis in Tibetan collisional orogenic belt: II. Mineralization in late-collisional transformation setting. Mineral Deposits 25, 521–543 (in Chinese with English abstract).

Hou, Z.Q., Khin, Z., Pan, G.T., Mo, X.X., Xu, Q., Hu, Y.Z., Li, X.Z., 2007. Sanjiang Tethyan metallogenesis in S.W. China: tectonic setting, metallogenic epochs and deposit types. Ore Geology Reviews 31, 48–87.

Ji, H.B., Li, C.Y., 1998. Geochemical characteristics and source of ore-forming fluid for Jinman copper deposit in western Yunnan Province, China. Acta Mineralogica Sinica 18, 28–37 (in Chinese with English abstract).

Kyle, J.K., Li, N., 2002. Jinding: a giant Tertiary sandstone-hosted Zn–Pb deposit, Yunnan, China. SEG. Newsletter 50, 8–16.

Leach, D.L., Sangster, D.F., Kelley, K.D., Large, R.R., Garven, G., Allen, C.R., Gutzmer, J., Walters, S., 2005. Sediment-hosted lead–zinc deposits: a global perspective. Economic Geology 100th Anniversary Volume, pp. 561–607.

Li, N., Kyle, J.K., 1997. Geologic controls of sandstone-hosted Zn–Pb–(Sr) mineralization, Jinding deposit, Yunnan Province, China—a new environment for sediment-hosted Zn–Pb deposits. In: Pei, R.F. (Ed.), Proceedings, 30th International Geological Congress, 9, pp. 67–82.

Li, F., Huang, D.Y., Fu, W.M., 1995. Metallogenic law of red-bed copper deposits of the Lanping-Simao basin, Yunnan, China. Geotectonica et Metallogenia 19, 322–335 (in Chinese with English abstract).

Li, F., Fu, W.M., Li, L., 1997. The material origin of the regional metallogenesis of copper deposits in red beds of west Yunnan. Journal of Yunnan Geology 16, 233–244 (in Chinese).

Li, X.Z., Liu, W.J., Wang, Y.Z., Zhu, Q.W., 1999. Tectonic Evolution of the Tethys and Mineralization in the Sanjiang Region, S.W. China. Geological Publishing House, Beijing. 258 pp. (in Chinese with English abstract).

Li, Z.M., Liu, J.J., Qin, J.Z., Liao, Z.T., Zhang, C.J., 2004. C, O and H isotopic compositions of polymetallic deposits in Lanping basin, western Yunnan Province and their geological significance. Journal of Jilin University (Earth Science Edition) 34, 360–366 (in Chinese with English abstract).

Li, Z.M., Liu, J.J., Qin, J.Z., Liao, Z.T., He, M.Q., Liu, Y.P., 2005. Ore-forming matieral source of the Baiyangping copper–cobalt–silver polymetallic deposit in Lanping basin, Western Yunnan. Geology and Prospecting 1, 1–6 (in Chinese with English abstract).

Li, Y.L., Wang, C.S., Yi, H.S., Liu, Z.F., Li, Y., 2006a. Cenozoic thrust system and uplifting of the Tanggula Mountain, Northern Tibet. Acta Geologica Sinica 80, 1118–1131 (in Chinese with English abstract).

Li, Y.G., Hou, Z.J., Wang, A.J., Tang, J.X., Liu, J.L., Xue, C.J., Xiu, Q.Y., 2006b. Geochemistry of Cenozoic detrital rocks and its constraints on provenance in Lanping basin. Acta Geologica Sinica 22, 751–760 (in Chinese with English abstract).

Liao, Z.T., Chen, Y.K., 2005. Nature and evolution of Lanping-Simao basin prototype. Journal of Tongji University (Nature Science) 33, 1528–1531 (in Chinese with English abstract).

Liu, Z.Q., Pan, G.T., Zheng, H.X., 1983. A preliminary study on the north boundary and the evolution of Gondwana and Tethys in light of the new data on Qinghai-Xizang (Tibet) Plateau. Committee of Geological Memoirs of Qinghai-Xizang. . Geological Memoirs of Qinghai-Xizang Plateau (12)-Geological Tectonics of "Sanjiang". Geological Publishing House, Beijing, pp. 11–24 (in Chinese).

Liu, Z.Q., Li, X.Z., Ye, Q.T., Luo, J.N., Shen, G.F., 1993. Division of Tectono-Magmatic Zones and the Distribution of Deposits in the Sanjiang Area. Geological Publishing House, Beijing. 246 pp. (in Chinese with English abstract).

Liu, J.J., Li, C.Y., Pan, J.Y., 2000. Isotopic geochemistry in the copper deposits from sandstone and shale in Lanping-Simao basin, western Yunnan. Mineral Deposits 19, 223–234 (in Chinese with English abstract).

Liu, J.J., Li, C.Y., Zhang, Q., 2001. Wood cell texture from Jinman copper deposit in west Yunnan and its genesis significance. Science in China (Series D) 32, 89–95 (in Chinese with English abstract).

Liu, J.J., Li, Z.M., Liu, Y.P., Li, C.Y., Zhang, Q., He, M.Q., Yang, W.G., Yang, A.P., Sang, H.Q., 2003. The metallogenic age of Jinman vein copper deposit, western Yunnan. Geoscience 17, 34–39 (in Chinese with English abstract).

Liu, J.J., He, M.Q., Li, Z.M., Liu, Y.P., Li, C.Y., Zhang, Q., Yang, W.G., Yang, A.P., 2004. Oxygen and carbon isotopic geochemistry of Baiyangping silver–copper polymetallic ore concentration area in Lanping basin of Yunnan province and its significance. Mineral Deposits, 23, 1–10 (in Chinese with English abstract).

Liu, J.L., Song, Z.J., Cao, S.Y., Zhai, Y.F., Wang, A.J., Gao, L., Xiu, Q.Y., Cao, D.H., 2006. The dynamic setting and processes of tectonic and magmatic evolution of the oblique collision zone between Indian and Eurasian plates: exemplified by the tectonic evolution of the Three River region, eastern Tibet. Acta Petrologica Sinica 4, 755–786 (in Chinese with English abstract).

Luo, J.L., Yang, Y.H., Zhao, Z.W., 1994. Evolution of the Tethys in Western Yunnan and Mineralization for Main Metal Deposits. Geological Publishing House, Beijing. 235 pp. (in Chinese with English abstract).

Misra, K.C., 2000. Understanding Mineral Deposits. Kluwer Academic Publishers, London. 845 pp.

Mo, X.X., Lu, F.X., Shen, S.Y., Zhu, Q.W., Hou, Z.Q., 1993. Volcanism and Metallogeny in the Sanjiang Tethys. Geological Publishing House, Beijing. 250 pp. (in Chinese with English abstract).

Please cite this article as: He, L., et al., Thrust-controlled, sediment-hosted, Himalayan Zn–Pb–Cu–Ag deposits in the Lanping foreland fold belt, eastern margin of Tibetan Plateau, Ore Geology Reviews (2008), doi:10.1016/j.oregeorev.2008.11.001

Mu, C.L., Wang, J., Yu, Q., Zhang, L.S., 1999. The evolution of the sedimentary basin in Lanping area during Mesozoic–Cenozoic. Mineral Petrology 19, 30–36 (in Chinese with English abstract).
O'Neil, J.R., Clayton, R.N., Mayeda, T.K., 1969. Oxygen isotope fractionation in divalent metal carbonates. Journal of Chemical Physics 51, 5547–5558.
Pan, G.T., Xu, Q., Hou, Z.Q., Wang, L.Q., Du, D.X., Mo, X.X., Li, D.M., Wang, M.J., Jiang, X.S., Hu, Y.Z., 2003. The ore-forming system of the orogenic processing in the western "Sangjiang" ploy-arc and the resources estimate. Geological Publishing House, Beijing. 420 pp. (in Chinese).
Pirajno, F., 1992. Hydrothermal Mineral Deposits. Springer-Verlag, Berlin. 708 pp.
Qin, G.J., Zhu, S.Q., 1991. Genetic model and prospecting prediction of Jinding Pb–Zn ore deposit. Journal of Yunan Geology 10, 145–190 (in Chinese).
Sangster, D.F., 1990. Mississippi Valley-type and Sedex lead–zinc deposits — a comparative examination. Institution of Mining and Metallurgy Transactions, Section B, Applied Earth Sciences 99, 21–42.
Shi, J.X., Yi, F.H., Wen, Q.D., 1983. The rock-ore characteristics and mineralization of Jinding lead–zinc deposit, Lanping. Journal of Yunnan Geology 2, 179–195 (in Chinese with English abstract).
Spurlin, M.S., Yin, A., Horton, B.K., Zhou, J.Y., Wang, J.H., 2005. Structural evolution of the Yushu-Nangqian region and its relationship to syncollisional igneous activity, east-central Tibet. GSA Bulletin 117, 1293–1317.
Sverjensky, D.A., 1986. Genesis of Mississippi Valley-type lead-zinc deposits. Annual Review of Earth and Planetary Sciences 14, 177–179.
Tapponnier, P., Lacassin, R., Leloup, P.H., 1990. The Ailao Shan–Red River metamorphic belt, Tertiary left lateral shear between Indochina and South China. Nature 343, 431–437.
Third Geological Surveying Party of Yunnan Geological and Mineral Resources Bureau, 1984. The Geological Exploration Report of Lead–zinc Ore Deposit in Lanping Country, Yunnan Province. Unpublished Report, Yunnan Geological and Mineral Resources Bureau, p. 101–105. (in Chinese).
Tian, H.L., 1997. The geological features of Baiyangping Cu–Ag polymetallic deposit, Lanping. Journal of Yunan Geology 16, 105–108 (in Chinese).
Wang, E., Burchfiel, B.C., 1997. Interpretation of Cenozoic tectonics in the right-lateral accommodation zone between the Ailao Shan shear zone and the eastern Himalayan syntaxis. International Geological Review 39, 191–219.
Wang, J.H., Yin, A., Harrison, T.M., Grove, M., Zhang, Y.Q., Xie, G.H., 2001. A tectonic model for Cenozoic igneous activities in the eastern Indo-Asian collision zone. Earth and Planetary Science Letters 188, 123–133.
Wang, F., He, M.Y., 2003. Lead and sulfur isotopic tracing of the ore forming material from the Baiyangping copper–silver polymetallic deposit in Lanping, Yunnan. Sedimentary Geology and Tethyan Geology 23, 82–85 (in Chinese with English abstract).
Wang, Y.B., Zeng, P.S., Li, Y.H., Tian, S.H., 2005. He–Ar isotopic composition of Jinding and Baiyangping mineral deposit and its significance. Mineral Petrology 24, 76–80 (in Chinese with English abstract).
Wang, A.J., Gao, L., Liu, J.L., Cao, D.H., Xiu, Q.Y., Fan, S.J., 2007. Genesis of the host breccia in the Lanping Jinding super-large Pb–Zn deposit. Acta Geologica Sinica 81, 891–897 (in Chinese with English abstract).
Wei, J.Q., 2001. S–Pb Isotopic geochemistry of copper multi-metal deposits in Hexi, Yunnan province. Geology and Mineral Resources of South China 3, 36–39 (in Chinese with English abstract).
Wu, N.P., Jiang, S.Y., Liao, Q.L., Pan, J.Y., Dai, B.Z., 2003. Lead and sulfur isotope geochemistry and the ore sources of the vein-type copper deposit in Lanping-Simao Basin, Yunan province. Acta Petrologica Sinica 19, 799–807 (in Chinese with English abstract).
Xiao, R.G., 1989. Reservation of Thermal Brine with Ore-forming Materials and Abrupt Mineralization. Unpublished Postdoctoral Report, Institute of Geochemistry, Chinese Academy of Sciences, Guiyang. 77 pp. (in Chinese).
Xiu, Q.Y., Wang, A.J., Gao, L., Liu, J.L., Yu, C.L., Cao, D.H., Zhai, Y.F., Fan, S.J., 2006. Discussion on the geologic time of host rocks of Jinding super large deposit and its geological implications. Geological Survey and Research 29, 293–302 (in Chinese with English abstract).
Xu, Q.D., Li, J.W., 2003. Migration of ore-forming fluids and its relation to zoning of mineralization in northern Lanping Cu-polymetallic area, Yunnan Province: evidence from fluid inclusions and stable isotopes. Mineral Deposits 22, 366–376 (in Chinese with English abstract).
Xu, Q.D., Zhou, L., 2004. Ore-forming fluid migration in relation to mineralization zoning in Cu-polymetallic mineralization district of northern Lanping, Yunnan: evidence from Lead isotope and mineral chemistry of ores. Mineral Deposits 23, 452–463 (in Chinese with English abstract).
Xu, X.C., Huang, Z., Xie, Q.Q., Yue, S.C., Liu, Y., 2004. Ar–Ar isotopic ages of Jinman and Shuixie copper polymetallic deposits in Yunnan Province. Geological Journal of China Universities 10, 157–164 (in Chinese with English abstract).
Xue, C.J., Chen, Y.C., Yang, J.M., Wang, D.H., 2002. Jinding Pb–Zn deposit: geology and geochemistry. Mineral Deposits 21, 270–277 (in Chinese with English abstract).
Xue, C.J., Liu, S.W., Chen, Y.C., 2003. Geology and isotopic composition of helium, neon, xenon and metallogenic age of the Jinding and Baiyangping ore deposits, northwest Yunnan, China. Science in China (series D) 46, 789–800 (in Chinese with English abstract).
Xue, C.J., Zeng, R., Liu, S.W., Chi, G.X., Qing, H.R., Chen, Y.C., Yang, J.M., Wang, D.H., 2007. Geologic, fluid inclusion and isotopic characteristics of the Jinding Zn–Pb deposit, western Yunnan, South China: a review. Ore Geology Reviews 31, 337–359.
Yan, W., 1993. Study on Geochemistry of a New Type Copper Deposit. Unpublished Dissertation for Master Degree, Institute of Geochemistry, Chinese Academy of Sciences, Guiyang. 87 pp. (in Chinese).
Yan, W., Li, Z.Y., 1997. Geochemical characteristics and their hydrothermal sedimentary genesis of a new type of copper deposit. Geochimica 26, 54–63 (in Chinese with English abstract).
Yang, W.G., 2002. Geological–Geochemical Conditions and Mechanism of Mineralization of Ag–Cu and Polymetallic Ore Deposits in Baiyangping, Lanping, Yunnan. Unpublished PhD. Dissertation, China University of Geosciences, 94 pp. (in Chinese with English abstract).
Yang, W.G., Yu, X.H., Li, W.C., Dong, F.L., Mo, X.X., 2003. The characteristics of metallogenic fluids and metallogenic mechanism in Baiyangping silver and polymetallic mineralization concentration area in Yunnan Province. Geoscience 17, 27–33 (in Chinese with English abstract).
Ye, Q.T., Hu, Y.Z., Yang, Y.Q., 1992. Regional Geochemistry Background and the Gold–Silver–Lead–Zinc Mineralization in Sanjiang Area. Geological Publishing House, Beijing, pp. 21–264 (in Chinese with English abstract).
Yin, A., Harrison, T.M., 2000. Geologic evolution of the Himalayan–Tibetan orogen. Annual Review of Earth and Planetary Sciences 28, 211–280.
Zhang, L.G., 1985. The Application of Stable Isotope to Geology. Shanxi Science and Technology Publishing House, Xi'an. 185 pp. (in Chinese).
Zhang, Q., 1993. Pb isotopic composition of Jinding super-large Pb–Zn in Yunnan Province and discussion on the sources of lead. Geology and Prospecting 29, 21–28 (in Chinese with English abstract).
Zhao, H.B., 2006. Study on the Characteristics and Metallogenic Condition of Copper-Polymetallic Deposits in Middle-northern Lanping Basin, Western Yunnan. Unpublished PhD. Dissertation, China University of Geosciences, 123 pp. (in Chinese with English abstract).
Zhong, D.L., Ding, L., Liu, F.T., Liu, J.H., Zhang, J.J., Ji, J.Q., Chen, H., 2000. Poly-layered architecture of lithosphere in orogen and its constraint on Cenozoic magmatism-example from Sanjiang and surrounding area. Science in China (Series D) 30 (S1), 1–8 (in Chinese).
Zhou, W.Q., Zhou, Q.L., 1992. A study on the isotopic composition of Pb and S in the Lanping Pb–Zn deposit, Yunnan Province. Geochimica 20, 141–148 (in Chinese with English abstract).

Please cite this article as: He, L., et al., Thrust-controlled, sediment-hosted, Himalayan Zn–Pb–Cu–Ag deposits in the Lanping foreland fold belt, eastern margin of Tibetan Plateau, Ore Geology Reviews (2008), doi:10.1016/j.oregeorev.2008.11.001